Supplementary Materials

Visualizing spatial population structure with estimated effective migration surfaces

D Petkova[1], J Novembre[2] & M Stephens[1,2]

[1] *Department of Statistics, University of Chicago*

[2] *Department of Human Genetics, University of Chicago*

Contents

S1 Supplementary Methods

Here is a summary of the sections in this supplement.

- In Supplementary Methods S1.1 we derive expressions for the expected genetic dissimilarities at a random marker, in terms of expected coalescence times.
- In Supplementary Methods S1.2 we derive an approximation for the expected genetic dissimilarities in a spatial (stepping stone) model, in terms of effective resistances in an undirected weighted graph.
- In Supplementary Methods S1.3 we explain how to compute efficiently the Wishart likelihood $\ell(k, m, q, \sigma^2)$ for the degrees of freedom k, the effective migration rates m, the effective diversity rates q and the variance scale σ^2.
- In Supplementary Methods S1.4 we explain how the effective resistances R in an undirected weighted graph can be computed efficiently, for the purpose of evaluating the likelihood $\ell(k, m, q, \sigma^2)$.
- In Supplementary Methods S1.5 we describe how to use birth-death Markov Chain Monte Carlo to sample from the posterior distribution $\pi(k, m, q, \sigma^2 \,|\, D)$.
- In Supplementary Methods S1.6 we discuss the color scheme used to present the estimated effective migration and diversity rates as colored contour plots.

S1.1 Expected genetic dissimilarities in population genetics

We derive the expected genetic dissimilarity between two distinct individuals i and j as a function of their expected coalescence time T_{ij}. In population genetics, expected coalescence time can be considered a distance metric: the larger T_{ij} is, the more differentiated i and j are, as they would not share mutations either lineage accumulates after the split from their most recent common ancestor (MRCA). We consider a randomly selected genetic marker l, either a SNP or a microsatellite, in a haploid or a diploid species. Let Z_{il} denote the genotype of individual i at locus l. Then the squared difference $(Z_{il} - Z_{jl})^2$ is a measure of the genetic dissimilarity between i and j at the locus l.

Expected dissimilarities at a random SNP in a haploid species

Suppose that SNP l is genotyped in a sample of size n. Following (McVean, 2009), we condition on the event S that the SNP segregates in the sample, and we take the limit $\theta \to 0$, where θ is the mutation rate. In a haploid species, $Z_{il} \in \{0, 1\}$ is the allele carried by individual i at SNP l and the event S is equivalent to observing exactly one mutation. The expected genetic difference $(Z_{il} - Z_{jl})^2$ is the probability that $Z_{il} \neq Z_{jl}$, and so

$$\mathrm{E}\Big\{(Z_{il} - Z_{jl})^2 \,|\, S\Big\} = \Pr\Big\{Z_{il} \neq Z_{jl} \,|\, S\Big\} = \Pr\{Z_{il} \neq Z_{jl}\} / \Pr\{S\} \tag{S1a}$$

$$= \lim_{\theta \to 0} \frac{\mathrm{E}\Big\{(\theta t_{ij}) \exp(-\theta t_{ij})\Big\}}{\mathrm{E}\Big\{(\theta t_{\mathrm{tot}}/2) \exp(-\theta t_{\mathrm{tot}}/2)\Big\}} = \frac{2T_{ij}}{T_{\mathrm{tot}}}, \tag{S1b}$$

where the t's are (random) coalescence times and the T's are their expectations, under the underlying genealogical process. For a given sample, T_{tot} is the expected total length (sum of all branches) of a random genealogy which describes the history of the entire sample back to its MRCA. For two haploid individuals i, j, the probability that they carry a different allele at a random SNP, $\Pr\{Z_{il} \neq Z_{jl}\}$, is proportional to $2T_{ij}$ because i and j carry different alleles if and only if a mutation occurs on the path from i to j through the pair's MRCA, which is of expected length $2T_{ij}$.

Expected dissimilarities at a random SNP in a diploid species

We model the genotype of a diploid individual i as the sum of two haplotypes i_1 and i_2. Thus $Z_{il} = Z_{i_1 l} + Z_{i_2 l} \in \{0, 1, 2\}$, where the subscript indicates one of two alleles. To derive the expected genetic dissimilarity between two distinct individuals i and j, we use the results from (McVean, 2009) that (conditioning on the event S and taking the limit $\theta \to 0$ as in the haploid case):

$$\mathrm{E}\Big\{Z_{i_1 l}^2 \,|\, S\Big\} = \mathrm{E}\Big\{Z_{i_1 l} \,|\, S\Big\} = T_{\mathrm{mrca}}/T_{\mathrm{tot}}, \tag{S2a}$$

$$\mathrm{E}\Big\{Z_{i_1 l} Z_{j_1 l} \,|\, S\Big\} = \Big(T_{\mathrm{mrca}} - T_{ij}\Big)/T_{\mathrm{tot}}, \tag{S2b}$$

where T_{mrca} denotes the expected coalescence time to the MRCA of all sampled individuals, i.e., the height of the average genealogy of the sample. By applying equations (S2a) and (S2b) repeatedly, we obtain:

$$\mathrm{E}\Big\{(Z_{il} - Z_{jl})^2 \,|\, S\Big\} = \mathrm{E}\Big\{\Big(Z_{i_1 l}^2 + Z_{i_2 l}^2 + Z_{j_1 l}^2 + Z_{j_2 l}^2\Big) + 2Z_{i_1 l} Z_{i_2 l} + 2Z_{j_1 l} Z_{j_2 l} - 2\Big(Z_{i_1 l} Z_{j_1 l} + Z_{i_1 l} Z_{j_2 l} + Z_{i_2 l} Z_{j_1 l} + Z_{i_2 l} Z_{j_2 l}\Big) \,|\, S\Big\}$$

$$= 4\frac{T_{\mathrm{mrca}}}{T_{\mathrm{tot}}} + 2\Big(\frac{T_{\mathrm{mrca}} - T_i}{T_{\mathrm{tot}}}\Big) + 2\Big(\frac{T_{\mathrm{mrca}} - T_j}{T_{\mathrm{tot}}}\Big) - 8\Big(\frac{T_{\mathrm{mrca}} - T_{ij}}{T_{\mathrm{tot}}}\Big) = 2\Big(\frac{4T_{ij} - T_i - T_j}{T_{\mathrm{tot}}}\Big), \tag{S3}$$

where $T_i = \mathrm{E}\{t_{i_1 i_2}\}$ and $T_j = \mathrm{E}\{t_{j_1 j_2}\}$ at a random SNP l.

Expected dissimilarities at a random microsatellite in a diploid species

At a microsatellite locus, an allele is coded as the "number of repeats" of a short DNA motif (two to six base pairs). The mutation process at this genetic variant can be modeled by a symmetric stepwise mechanism where the number of repeats increases or decreases by 1, with equal probability (Ohta and Kimura, 1973).

We model the genotype Z_{il} of a diploid individual at microsatellite l as the average of the two alleles, $Z_{i_1 l}$ and $Z_{i_2 l}$. Under the symmetric mutation process,

$$Z_{i_1 l} = a_l + \sum_{k=1}^{K_{i_1 l}} S_k, \tag{S4}$$

where a_l is the ancestral allele at microsatellite l (the allele carried by the MRCA of all lineages in the sample), $K_{i_1 l}$ denotes the number of mutations that occur on the lineage from haplotype i_1 to the MRCA, and the S_ks are independent binary random variables with $\Pr\{S_k = 1\} = \Pr\{S_k = -1\} = \frac{1}{2}$.

Let θ_l denote the mutation rate at microsatellite l. If we assume that the mutations S_k at marker l occur as a Poisson process with mutation rate θ_l, then $K_{i_1 l} \,|\, \theta_l, t_{\text{mrca}} \sim \text{Po}(\theta_l t_{\text{mrca}})$ (Hudson, 1990). Thus, we have:

$$\begin{aligned} \text{E}\Big\{Z_{i_1 l}^2 \,|\, \theta_l\Big\} &= a_l^2 + \text{E}\Big\{\text{E}\Big\{\Big(\sum_{k=1}^{K_{i_1 l}} S_k\Big)^2 \,|\, t_{\text{mrca}}\Big\} \,|\, \theta_l\Big\} = a_l^2 + \text{E}\Big\{\text{E}\Big\{\sum_{k=1}^{K_{i_1 l}} S_k^2 \,|\, t_{\text{mrca}}\Big\} \,|\, \theta_l\Big\} \\ &= a_l^2 + \text{E}\Big\{\text{E}\Big\{K_{i_1 l} \,|\, t_{\text{mrca}}\Big\} \,|\, \theta_l\Big\} = a_l^2 + \text{E}\Big\{\theta_l t_{\text{mrca}} \,|\, \theta_l\Big\} = a_l^2 + \theta_l T_{\text{mrca}}. \end{aligned} \tag{S5}$$

(We have used: $\text{E}\{Z_{i_1 l}\} = a_l + \sum_k S_k = a_l$ and $\text{E}\{S_k S_{k'}\} = 0$ since the S_ks have mean 0, variance 1 and are independent.) Similarly,

$$\text{E}\Big\{Z_{i_1 l} Z_{j_1 l} \,|\, \theta_l\Big\} = a_l^2 + \theta_l\Big(T_{\text{mrca}} - T_{ij}\Big). \tag{S6}$$

Now we can combine equations (S5) and (S6) to obtain:

$$\text{E}\Big\{(Z_{il} - Z_{jl})^2 \,|\, \theta_l\Big\} = \frac{\theta_l}{2}\Big(4T_{ij} - T_i - T_j\Big). \tag{S7}$$

Compared to equation (S3), there is a factor of 1/4 because we model a diploid genotype at a microsatellite locus as the *average* of two alleles rather than the *sum* of two alleles, as in the case of SNPs.

S1.2 Expected genetic dissimilarities in EEMS

EEMS is based on the stepping stone model (Kimura and Weiss, 1964), which specifies that the expected coalescence times between two distinct individuals depends only on their locations:

$$T_{ij} = T_{\delta(i)\delta(j)}, \tag{S8}$$

for individuals i and j drawn randomly from demes $\delta(i)$ and $\delta(j)$, respectively.

Let D be the matrix of observed genetic differences: $D = (D_{ij}) = \Big((Z_{il} - Z_{jl})^2\Big)$ at a randomly selected (polymorphic) genetic marker l. If $i = j$, both the observed and the expected dissimilarity with self is 0. If $i \neq j$, the expected genetic dissimilarity is given by equations (S1), (S3) and (S7):

$$\text{E}\{D_{ij} \,|\, *\} = \begin{cases} \sigma^2 T_{\delta(i)\delta(j)}, \text{ hap/SNP}; & \sigma^2\Big(4T_{\delta(i)\delta(j)} - T_{\delta(i)} - T_{\delta(j)}\Big), \text{ dip/SNP}; \\ \sigma_l^2 T_{\delta(i)\delta(j)}, \text{ hap/sat } l; & \sigma_l^2\Big(4T_{\delta(i)\delta(j)} - T_{\delta(i)} - T_{\delta(j)}\Big), \text{ dip/sat } l; \end{cases} \tag{S9}$$

where the symbol $*$ indicates the event that the site segregates in the sample (if the marker is a SNP), and the mutation rate θ_l (if the locus is a microsatellite). The constant of proportionality is $2/T_{\text{tot}}$ for SNPs and $\theta_l/2$ for microsatellites, which we write σ^2 and σ_l^2, respectively, because the size of the average sample genealogy T_{tot} and the mutation rate θ_l are not of interest in EEMS.

Therefore, as a direct consequence of equation (S8), the expected genetic dissimilarity between two distinct individuals depends only on their locations. That is, EEMS assumes that individuals in the same deme are exchangeable.

EEMS decomposes genetic dissimilarities into between-demes and within-demes components

Consider two different demes α and β. Suppose that individual i is assigned to deme α, which we denote by $\delta(i) = \alpha$. Similarly, suppose that $\delta(i^*) = \alpha$ but i and i^* are distinct individuals, that $\delta(j) = \beta$ and $\delta(j^*) = \beta$ but j and j^* are distinct individuals. [Of course, i and j are distinct because they come from different demes.]

EEMS is a spatially explicit model and it is consistent with the following idea: We can expect that $\langle i, j\rangle$ are more dissimilar than either $\langle i, i^*\rangle$ or $\langle j, j^*\rangle$ because i and j come from different locations. However, in general, we can't expect $\langle i, i^*\rangle$ to be as dissimilar as $\langle j, j^*\rangle$ – there might be some differences in local genetic diversity. And to model the genetic dissimilarity due to migration in space we should take into account any local variation in genetic diversity.

To capture this idea, EEMS approximates the expected coalescence time between two distinct demes α and β by splitting $T_{\alpha\beta}$ into two components:

$$T_{\alpha\beta} \;=\; \underbrace{T_{\alpha\beta} - \Big(T_\alpha + T_\beta\Big)/2}_{\text{between demes}} + \underbrace{\Big(T_\alpha + T_\beta\Big)/2}_{\text{within demes}} \;\approx\; R_{\alpha\beta}/4 + \Big(q_\alpha + q_\beta\Big)/2, \tag{S10}$$

where $R_{\alpha\beta}$ is the resistance distance between demes (vertices) α and β in the undirected, connected population grid, and q_α, q_β are the effective diversity rates at α and β, respectively. In this approximation, resistance distances specify the expected genetic differentiation between distinct demes in the habitat (the between-demes component), while the effective diversity rates specify the expected genetic differentiation between distinct individuals from the same deme (the within-demes component).

EEMS uses the approximation given by equation (S10) to specify a model for the expected genetic dissimilarities:

$$\mathrm{E}\{D_{ij} \,|\, *\} \approx \begin{cases} \sigma^2\Big(R_{\delta(i)\delta(j)}/4 + (q_{\delta(i)} + q_{\delta(j)})/2\Big), \text{ hap/SNP}; & \sigma^2\Big(R_{\delta(i)\delta(j)} + (q_{\delta(i)} + q_{\delta(j)})\Big), \text{ dip/SNP}; \\ \sigma_l^2\Big(R_{\delta(i)\delta(j)}/4 + (q_{\delta(i)} + q_{\delta(j)})/2\Big), \text{ hap/sat } l; & \sigma_l^2\Big(R_{\delta(i)\delta(j)} + (q_{\delta(i)} + q_{\delta(j)})\Big), \text{ dip/sat } l; \end{cases} \tag{S11a}$$

$$\propto \quad B_{\delta(i)\delta(j)} + (w_{\delta(i)} + w_{\delta(j)})/2 \quad \text{in all four cases.} \tag{S11b}$$

In matrix notation $\mathrm{E}\{D \,|\, *\} \propto \Delta$ and the constant of proportionality is σ^2 for SNPs and σ_l^2 for microsatellite l. Furthermore, the expected dissimilarity matrix Δ has the same form in all four cases, and for the purpose of generality, we can write

$$\Delta = JBJ' + \tfrac{1}{2}Jw1_n' + \tfrac{1}{2}1_n w'J' - W_n, \tag{S12}$$

where $B = (B_{\alpha\beta})$ is the matrix of between-deme dissimilarities, $w = (w_\alpha)$ is the vector of within-demes dissimilarities, $J = (J_{i\alpha})$ is an indicator matrix such that $J_{i\alpha} = 1$ if individual i comes from deme α, and

$W_n = \mathrm{diag}\{Jw\}$. We subtract the diagonal matrix $W_n = \mathrm{diag}\{\frac{1}{2}Jw1'_n + \frac{1}{2}1_n w'J'\}$ because the expected dissimilarity matrix Δ has a main diagonal of 0s. If there are n individuals sampled from o demes, then $J \in \mathbb{Z}^{n\times o}$, $B \in \mathbb{R}^{o\times o}$, $w \in \mathbb{R}^o$. To simplify the notation, we drop the subscripts and write plainly 1 for the vector of 1s. The dimension will be clear from the context because B is an $o \times o$ matrix and Δ is an $n \times n$ matrix.

EEMS models between-demes dissimilarities in terms of migration and within-demes dissimilarities in terms of diversity

The within-demes component w characterizes the expected genetic dissimilarity between two distinct individuals from the same deme and is a function of the effective diversity rates:

$$w_\alpha = g(q_\alpha). \tag{S13}$$

Here q is a vector of effective diversity rates and q_α is the element that corresponds to deme α. The function g is the identity.

The between-demes component B characterizes the expected genetic dissimilarity between two individuals from distinct demes, *after* correcting for the local differences in genetic diversity, and is a function of the effective migration rates:

$$B_{\alpha\beta} = f(m)_{\alpha\beta}. \tag{S14}$$

Here m is a sparse matrix that represents an undirected, connected, weighted grid, with weights equal to the effective migration rates between adjacent demes. The function f returns the effective resistance distances between vertices in the grid, as a dense matrix, and $f(m)_{\alpha\beta}$ is the element which corresponds to the pair of demes α and β.

In EEMS model the parameters of the model are of greater interest than the expected dissimilarities, i.e., m and q are more interesting than the deterministic functions $f(m)$ and $g(q)$.

S1.3 Computing the Wishart likelihood in EEMS

EEMS represents the population as a connected undirected graph (V, E), with effective migration rates $m = \{(\alpha, \beta) \in E : m_{\alpha\beta}\}$ and effective diversity rates $q = \{\alpha \in V : q_\alpha\}$. Furthermore, EEMS models the observed genetic differences D between n individuals, averaged across p SNPs, through a positive definite transformation:

$$-LDL' \,|\, k, m, q, \sigma^2 \sim \mathrm{W}_{n-1}\Big(k, -\frac{\sigma^2}{k} L\Delta(m, q)L'\Big), \tag{S15}$$

where $\Delta(m, q)$ is the matrix of expected genetic dissimilarities as function of the between-demes component $B(m)$ and the within-demes component $w(q)$. [In Supplementary Methods S1.2, Δ is given by equation (S12), w by Equation (S13) and B by Equation (S14).] In addition, L is a $(n-1)\times n$ basis for contrasts on n elements, k is the degrees of freedom, constrained to lie in the range $[n, p]$, and σ^2 is a scale parameter. See Supplementary Methods S1.2 for a demographic interpretation of σ^2.

By definition, a contrast is a linear combination with coefficients that add to zero, so $L1 = 0$ and

$$L\Delta L' = L\Big(JBJ' + \tfrac{1}{2}Jw1' + \tfrac{1}{2}1w'J' - W_n\Big)L' = L\Big(JBJ' - W_n\Big)L'. \tag{S16}$$

Equation (S16) implies that Δ and $JBJ' - W_n$ are equivalent under the Wishart likelihood (S15) because they give the same likelihood. Therefore, without loss of generality, we can assume that the expected dissimilarity matrix has the form:

$$\Delta = JBJ' - W_n, \tag{S17}$$

where JBJ' is a block matrix and W_n is a diagonal matrix. We can exploit this structure to compute the Wishart log likelihood efficiently, without explicitly constructing the $n \times n$ matrix Δ. As a result, the computational cost scales with the grid size, not with the number of samples. The hard-to-compute terms of the Wishart likelihood (S15) are the determinant and the trace:

$$\operatorname{tr}\left\{(L\Delta L')^{-1}LDL'\right\} = \operatorname{tr}\left\{\Delta^{-1}\Big(\Delta L'(L\Delta L')^{-1}L\Big)D\right\} = \operatorname{tr}\left\{\Delta^{-1}QD\right\}, \tag{S18a}$$

$$\det\left\{-(L\Delta L')^{-1}\right\} = \det\left\{-L'(L\Delta L')^{-1}L\right\} / \det\left\{LL'\right\} = \operatorname{Det}\left\{-\Delta^{-1}Q\right\} / \det\left\{LL'\right\}, \tag{S18b}$$

where det denotes the standard determinant (the product of all eigenvalues), Det denotes the pseudo determinant (the product of the nonzero eigenvalues) and

$$Q = \Delta L'(L\Delta L')^{-1}L = I - 1(1'\Delta^{-1}1)^{-1}1'\Delta^{-1} \tag{S19}$$

is an orthogonal projection matrix with kernel $\{1\}$, the space of constant functions.

The distance matrix $\Delta = JBJ' - W_n$ is the sum of a block matrix and a diagonal matrix, and its inverse Δ^{-1} has similar "almost-block" structure:

$$\Delta^{-1} = JXJ' - W_n^{-1}, \tag{S20}$$

where X is an unknown $o \times o$ matrix. Since $\Delta\Delta^{-1} = I$, the solution X must satisfy:

$$JBCXJ' - W_nJXJ' - JBJ'W_n^{-1} + W_nW_n^{-1} = I \qquad \Leftrightarrow \qquad J(BC - W_o)XJ' = JBW_o^{-1}J', \tag{S21}$$

where $C = J'J = \operatorname{diag}\{n_\alpha\}$ is the diagonal matrix of deme sizes and n_α is the number of geo-referenced individuals assigned to deme α in the population graph. [Demes with $n_\alpha > 0$ are the observed demes.] Since every term in equation (S21) has exact block structure which depends on the sample configuration through J, it is sufficient to solve the lower-dimensional problem:

$$\Big(BC - W_o\Big)X = BW_o^{-1}. \tag{S22}$$

This is a system of linear equations for the unknown matrix X as a function of the between-demes dissimilarities B, the within-demes dissimilarities $W_o = \operatorname{diag}\{w\}$ and the sample counts C. Equation (S22) can be solved efficiently without a matrix inversion, by performing the LU factorization of $Y = BC - W_o$.

We can express the pseudo-determinant $\operatorname{Det}\{-\Delta^{-1}Q\}$ and the trace $\operatorname{tr}\{\Delta^{-1}QD\}$ in terms of the auxiliary matrix X. Using the definition of the orthogonal projection Q in equation (S19) and the properties of the trace,

$$\operatorname{tr}\left\{\Delta^{-1}QD\right\} = \operatorname{tr}\left\{\Delta^{-1}D\right\} - \frac{1}{1'\Delta^{-1}1}\operatorname{tr}\left\{11'\Delta^{-1}D\Delta^{-1}\right\}. \tag{S23}$$

For simplicity of notation, let $c = \mathrm{diag}\{C\}$ and $v = (w_\alpha^{-1})$. We consider each term in Equation (S23):

$$1'\Delta^{-1}1 = 1'\Big(JXJ' - W_n^{-1}\Big)1 = c'\Big(Xc - v\Big), \tag{S24a}$$

$$\mathrm{tr}\Big\{\Delta^{-1}D\Big\} = \mathrm{tr}\Big\{\Big(JXJ' - W_n^{-1}\Big)D\Big\} = \mathrm{tr}\Big\{XJ'DJ\Big\}, \tag{S24b}$$

$$\mathrm{tr}\Big\{11'\Delta^{-1}D\Delta^{-1}\Big\} = \Big(c'X'J' - v'J'\Big)D\Big(JXc - Jv\Big) = \Big(Xc - v\Big)'J'DJ\Big(Xc - v\Big). \tag{S24c}$$

The matrix product in red, $J'DJ$, is a known matrix of order o, where o is the number of observed demes, and it can be precomputed and stored for easy access. Thus we do not need to construct the $n \times n$ matrix Δ^{-1} in order to compute $\mathrm{tr}\{\Delta^{-1}QD\}$; we can work with the $o \times o$ matrix X instead. [It follows that the computational cost scales with the grid size, not with the sample size.]

Next we show how to compute the pseudo determinant $\mathrm{Det}\{-\Delta^{-1}Q\}$. Following (Verbyla, 1990), we can show that

$$\mathrm{Det}\Big\{-\Delta^{-1}Q\Big\} = \frac{\det\{LL'\}}{\det\{-L\Delta L'\}} = \frac{(1'1)/(1'\Delta^{-1}1)}{-\det\{-\Delta\}}. \tag{S25}$$

A distance matrix is conditionally negative definite, and so Δ has one positive eigenvalue and $n-1$ negative eigenvalues (Bapat and Raghavan, 1997). This guarantees that $-\det\{-\Delta\}$ is positive and so it is sufficient to compute $|\det\{\Delta\}| = |JBJ' - W_n|$, which can be obtained from the LU decomposition of $Y = BC - W_o$:

$$\Big|\det\{\Delta\}\Big| = \Big|\det\{W_n\}(-1)^{n-o}\det\{W_o^{-1}BC - I\}\Big| = \Big|\det\{W_n\}\det\{W_o^{-1}\}\det\{BC - W_o\}\Big|. \tag{S26}$$

We can use Equations (S24), (S25) and (S26) to evaluate the the Wishart likelihood (S15) for the parameters k, m, q and σ^2.

S1.4 Computing resistance distances in an undirected graph

In Supplementary Methods S1.3 the between-demes component $B(m)$ is the matrix of pairwise distances between demes. Various distance metrics can be considered but, following (McRae, 2006), EEMS uses the metric "effective resistance" or "resistance distance" $R(m)$.

Let $\mathcal{L}$ be the graph Laplacian of the population graph (V, E) with effective migration rates m. (Resistance distances do not depend on the diversity rates q, so those parameters are not relevant for the following computation.) The graph Laplacian is given by:

$$\mathcal{L} = \mathcal{D} - M, \tag{S27}$$

where $M = (m_{\alpha\beta})$ is the (sparse) matrix of effective migration rates between connected demes and $\mathcal{D} = (\mathcal{D}_{\alpha\alpha})$ is the diagonal matrix with $\mathcal{D}_{\alpha\alpha} = \sum_{\beta:\beta\neq\alpha} m_{\alpha\beta}$.

Following (Babić et al., 2002), we can use $\mathcal{L}$ to compute the effective resistances $R = (R_{\alpha\beta})$ for all pairs of demes in the population graph, by inverting the sum matrix $\Gamma = \mathcal{L} + 11'/c$ where $c > 0$ is a constant. Let $H = \Gamma^{-1}$ and $h = \mathrm{diag}\{H\}$. Then

$$R = 1h' + h1' - 2H. \tag{S28}$$

Importantly, equation (S16) suggests that we can take $B = -2H$ instead of $B = R$ because the matrices $-2H$ and R produce the same likelihood for the EEMS parameters and are therefore equivalent. In Supplementary

Methods S1.3 we use a similar argument to show that $\Delta = JBJ' + \frac{1}{2}Jw1' + \frac{1}{2}1w'J' - W_n$ and $JBJ' - W_n$ are equivalent under the Wishart likelihood (S15). In other words, the likelihood is invariant to adding components with the form $1v'$ or $v1'$ for a vector v.

Furthermore, we can avoid inverting the matrix Γ to obtain the auxiliary matrix X in equation (S20). [Γ is an $d \times d$ matrix where d is the number of demes in the graph; X is an $o \times o$ matrix where o is the number of demes assigned at least one individual.] Let $\Gamma_{o\times o}$ be the $o \times o$ block that corresponds to the observed demes; similarly, let $\Gamma_{(d-o)\times(d-o)}$ be the $(d-o) \times (d-o)$ block that corresponds to the unobserved demes. Then

$$H^{-1}_{o\times o} = \Gamma_{o\times o} - \Gamma_{o\times(d-o)}\Gamma^{-1}_{(d-o)\times(d-o)}\Gamma_{(d-o)\times o}, \tag{S29}$$

which can be computed efficiently by solving a linear system. Finally, the dissimilarities $B_{o\times o}$ between observed demes can be computed from $B^{-1}_{o\times o} = -H^{-1}_{o\times o}/2$. If the population graph is sparsely sampled, as is often the case, it is more efficient to compute the Schur complement of $\Gamma_{o\times o}$ in equation (S29), rather than invert the full-size matrix Γ. This idea is also used in (Hanks and Hooten, 2013).

Computational complexity

The auxiliary matrix Γ is dense, diagonally dominant, positive definite and of order d, where d is the number of observed demes. First we compute the Schur complement $H^{-11}_{o\times o}$ according to equation (S29), and then the between-demes dissimilarities $B_{o\times o}$.

1. Cholesky decomposition $\Gamma_{(d-o)\times(d-o)} = U'U$: $O((d-o)^3)$
2. Forward substitution $U'Y = \Gamma_{(d-o)\times o}$: $O(o(d-o)^2)$
3. Backward substitution $UX = Y$: $O(o(d-o)^2)$
4. Matrix inversion $B_{o\times o} = -H^{-1}_{o\times o}/2$: $O(o^3)$

This procedure has complexity $O((d+o)(d-o)^2 + o^3)$ and, except for very small graphs, it is more efficient than inverting the sum matrix Γ which has complexity $O(d^3)$.

S1.5 Birth-death Markov Chain Monte Carlo estimation

In Supplementary Methods S1.3 we assume, without loss of generality, that the expected dissimilarity matrix has the form:

$$\Delta(m, q) = JB(m)J' - W(q), \tag{S30}$$

where $B(m)$ is the between-demes component, which is a function of the migration rates m, and $W(q)$ is the within-demes component, which is a function the diversity rates q.

EEMS uses two Voronoi tessellations, which independently partition the habitat: one parametrizes the effective migration rates m, and the other – the effective diversity rates q. Specifically, the migration rates m are determined by a Voronoi tessellation with C_m cells, seeds $s_1, \ldots, s_{C_m}$, migration effects $e_1, \ldots, e_{C_m}$, and overall migration rate (on the $\log_{10}$ scale) μ, while the diversity rates are determined by another independent

Voronoi tessellation with C_q cells, seeds $t_1, \ldots, t_{C_q}$, and diversity effects $f_1, \ldots, f_{C_q}$. The overall diversity rate is assumed to be 0 on the $\log_{10}$ scale (1 on the original scale). We fix the overall diversity rate because the two components of the expected dissimilarity matrix scale so that $B(m/2) = 2B(m)$, $W(2q) = 2W(q)$. With the current parametrization, fixing the overall diversity rate to 1 makes the scale σ^2 identifiable. Finally, the migration cell effects $e_1, \ldots, e_{C_m}$, have variance ω_m^2, while the diversity cell effects $f_1, \ldots, f_{C_q}$ have variance ω_q^2.

We use birth-death Markov Chain Monte Carlo (MCMC) to estimate the number of cells C in each Voronoi tessellation because the dimension of the seeds and the cell effects changes as C increases or decreases. [The same procedure is used to update the migration and the diversity Voronoi tessellations, so instead of C_m or C_q we write C.] In each step, we propose the birth (addition) or death (removal) of a cell, with equal probability (Stephens, 2000). For a birth proposal, the acceptance probability is

$$\alpha(\Theta, \Theta^*) = \min\left\{1, u\frac{c+r}{c+1}\frac{\ell(\Theta^*)}{\ell(\Theta)}\right\}, \tag{S31}$$

where c is the current number of cells; (r, u) are the parameters of the negative binomial prior on C, Θ is the current parameter state (with c cells) and Θ^* is the proposed parameter state, with one additional cell added at a random location within the habitat and assigned a random effect drawn from a (truncated) normal prior. Small probability of success u means small acceptance probability α unless the likelihood ratio indicates strong evidence in favor of adding the new cell.

For a death proposal, one cell is randomly chosen to be removed. There should be at least one cell in the Voronoi tessellation at each step, so let $c + 1$ be the current number of cells, i.e., there are at least two cells currently. The acceptance probability for a death proposal has the form:

$$\alpha(\Theta, \Theta^*) = \min\left\{1, \frac{1}{u}\frac{c+1}{c+r}\frac{\ell(\Theta^*)}{\ell(\Theta)}\right\}. \tag{S32}$$

For SNP data, the parameter state $\Theta = (k, m, q, \sigma^2)$ consists of the degrees of freedom k, the migration rates m, the diversity rates q and a scale parameter σ^2; the likelihood $\ell(\Theta)$ is given by equation (3). For microsatellite data, the parameter state $\Theta = (m, q, \sigma_1^2, \ldots, \sigma_p^2)$ consists of the migration rates m, the diversity rates q and locus-specific scale parameters $\sigma_1^2, \ldots, \sigma_p^2$; the likelihood $\ell(\Theta)$ is given by equation (7).

For a given number of Voronoi cells C_m and C_q in the two Voronoi tessellations, the cell effects and their locations, the overall migration rate μ and (for SNPs data only) the effective degrees of freedom k are each updated in turn with a random-walk Metropolis-Hastings step:

$$\alpha(\Theta, \Theta^*) = \min\left\{1, \frac{p(\Theta^*)}{p(\Theta)}\frac{\ell(\Theta^*)}{\ell(\Theta)}\right\}, \tag{S33}$$

where $p(\Theta)$ is the prior and $\ell(\Theta)$ is the likelihood.

Finally, the scalar variance parameters are $\omega_m^2, \omega_q^2, \sigma^2$ for SNP data, and $\omega_m^2, \omega_q^2, \sigma_1^2, \ldots, \sigma_p^2$ for microsatellite data. These parameters are updated with a Gibbs step by sampling from the corresponding full conditional distribution, which is inverse gamma. For example, the variance in relative migration among cells, ω_m^2, is drawn from

$$\omega_m^2 \,|\, C, e_1 \ldots, e_C \sim \text{Inv-G}\Big((c_\omega + C)/2, (d_\omega + SS_e)/2\Big), \tag{S34}$$

where the sum of squares is $SS_e = \sum_{c=1}^{C} e_c$.

S1.6 Visualizing rate estimates as smooth contour plots

To simplify comparisons, we plot relative migration rates on the same scale throughout the paper; the blue-and-orange color palette is based a collection of divergent color schemes suitable for people with deficient red-green vision. As with any plot of this nature, the choice of color and scaling can affect – sometimes profoundly – the resulting image and the message it conveys. At the simplest level, a scheme that is too broad will wash-out any differences in effective migration rate between regions, while a scheme that is too narrow will risk over-emphasizing trivial differences. The color scheme used here, as well as some alternatives, is available at `http://geog.uoregon.edu/datagraphics/color_scales.htm` (Light and Bartlein, 2004).

An estimated effective migration surface (EEMS) is a colored contour plot. To create the plot:

1. Choose a grid of interpolation points (x, y) for the contour plot. The interpolation points do not correspond to the demes in the population graph, and we would choose a dense grid of interpolation points to obtain a smooth migration surface.

2. Compute the effective migration rate, $\log_{10}(m_{xy})$, at each interpolation point, from the estimated Voronoi tessellation of the effective migration rates. The Voronoi tessellation partitions the habitat, and each interpolation point is assigned the rate of the cell c which it falls into, $\log_{10}(m_c)$.

3. Standardize the migration rates, so that the mean over the interpolation points is 0.

The Voronoi cells do not necessarily have the same area, and so a different number of interpolation points would fall in each cell. Therefore, the unweighted average over the interpolation points corresponds to a weighted average across the Voronoi cells, with weights proportional to the area of each cell. This is the reason we do not use the estimate of the overall migration μ to standardize the interpolated rates for plotting. [Since $\log_{10}(m_c) = \mu + e_c$ for cell c, the overall migration rate μ is the unweighted mean over the cells. With the normalization described above, the "average color" across the colored contour plot is white.]

References

Auton, A. *et al.* (2009). Global distribution of genomic diversity underscores rich complex history of continental human populations. *Genome Res.*, 19:795–803.

Babić, D., Klein, D., Lukovits, I., Nikolić, S. & Trinajstić, N. (2002). Resistance-distance matrix: a computational algorithm and its application. *Int. J. Quantum. Chem.*, 90:166–176.

Bapat, R. B. & Raghavan, T. E. S. (1997). *Nonnegative matrices and applications*. Cambridge University Press, Cambridge, UK.

Comstock, K. *et al.* (2002). Patterns of molecular genetic variation among African elephant populations. *Mol. Ecol.*, 11:2489–2498.

Guillot, G., Estoup, A., Mortier, F. & Cosson, J. F. (2005). A spatial statistical model for landscape genetics. *Genetics*, 170:1261–1280.

Hanks, E. & Hooten, M. (2013). Circuit theory and model-based inference for landscape connectivity. *J. Am. Stat. Assoc.*, 108:22–33.

Henn, B. *et al.* (2011). Hunter-gatherer genomic diversity suggests a southern African origin for modern humans. *Proc. Natl. Acad. Sci. U.S.A.*, 108:5154–5162.

Horton, M. *et al.* (2012). Genome-wide patterns of genetic variation in worldwide *Arabidopsis thaliana* accessions from the RegMap panel. *Nat. Genet.*, 44:212–216.

Hubisz, M., Falush, D., Stephens, M. & Pritchard, J. (2009). Inferring weak population structure with the assistance of sample group information. *Mol. Ecol. Resour.*, 9:1322–1332.

Hudson, R. (1990). Gene genealogies and the coalescent process. In Futuyma, D. & Antonovics, J., editors, *Oxford surveys in evolutionary biology*, volume 7, pages 1–44. Oxford University Press.

Kimura, M. & Weiss, G. (1964). The stepping stone model of population structure and the decrease of genetic correlation with distance. *Genetics*, 49:561–576.

Lao, O. *et al.* (2008). Correlation between genetic and geographic structure in Europe. *Curr. Biol.*, 18:1241–1248.

Light, A. & Bartlein, P. (2004). The end of the rainbow? Color schemes for improved data graphics. *Eos*, 85:385.

McRae, B. (2006). Isolation by resistance. *Evolution*, 60:1551–1561.

McVean, G. (2009). A genealogical interpretation of principal components analysis. *PLoS Genet.*, 5:e1000686.

Nelson, M. *et al.* (2008). The population reference sample, POPRES: A resource for population, disease, and pharmacological genetics research. *Am. J. Hum. Genet.*, 83:347–358.

Novembre, J. *et al.* (2008). Genes mirror geography within Europe. *Nature*, 456:98–101.

Ohta, T. & Kimura, M. (1973). A model of mutation appropriate to estimate the number of electrophoretically detectable alleles in a finite population. *Genet. Res.*, 22:201–204.

Pemberton, T., Wang, C., Li, J. & Rosenberg, N. (2010). Inference of unexpected genetic relatedness among individuals in HapMap Phase III. *Am. J. Hum. Genet.*, 87:457–464.

Platt, A. *et al.* (2010). The scale of population structure in *Arabidopsis thaliana*. *PLoS Genet.*, 6:e1000843.

Pritchard, J., Stephens, M. & Donnelly, P. (2000). Inference of population structure using multilocus genotype data. *Genetics*, 155:945–959.

Stephens, M. (2000). Bayesian analysis of mixture models with an unknown number of components —an alternative to reversible jump methods. *Ann. Stat.*, 28:40–74.

Verbyla, A. P. (1990). A conditional derivation of residual maximum likelihood. *Aust. J. Stat.*, 32:227–230.

Wang, C., Zöllner, S. & Rosenberg, N. (2012). A quantitative comparison of the similarity between genes and geography in worldwide human populations. *PLoS Genet.*, 8:e1002886.

Wasser, S. *et al.* (2004). Assigning African elephant DNA to geographic region of origin: Applications to the ivory trade. *Proc. Natl. Acad. Sci. U.S.A.*, 10:14847–14852.

Wasser, S. K. *et al.* (2015). Genetic assignment of large seizures of elephant ivory reveals Africa's major poaching hotspots. *Science*, 349:84–87.

Xing, J. *et al.* (2010). Toward a more uniform sampling of human genetic diversity: A survey of worldwide populations by high-density genotyping. *Genomics*, 96:199–210.

S2 Supplementary Tables

List of Supplementary Tables

Population	Symbol	Size	Comment about sample exclusions
Austria	AT	14	
Belgium	BE	43	
Denmark	DK	1	
France	FR	89	
Germany	DE	71	
Ireland	IE	61	
Italy	IT	214(219)	Removed 7623, 33242, 34049, 38532, 49500 as PCA outliers.
Netherlands	NL	17	
Portugal	PT	128	
Scotland	Sct	5	
Spain	ES	136	
Swiss-French	CHf	125	
Swiss-German	CHg	84	
Swiss-Italian	CHi	13	
United Kingdom	UK	200	

Supplementary Table 1 Description of the Western Europe dataset, which is a subset of data analyzed in (Novembre et al., 2008). It comprises 15 populations from 13 countries; their names and abbreviations, which generally correspond to ISO country codes, are given in the first and second column. The samples from Switzerland (CH) are split into three subpopulations: French, Italian and German speaking Swiss, coded as CHf, CHi and CHg, respectively. The number of samples from each population are given in the third column. We excluded five individuals as possible outliers based on their position in PC1-PC2 space: they project outside of the main Italian cluster and thus might have insular Italian ancestry – Sardinian or Sicilian (Novembre et al., 2008).

Population	Symbol	Size	Dataset	Comment about sample exclusions
Alur	Al	10	(Xing et al., 2010)	
Bambaran	Ba1	25	(Xing et al., 2010)	
Bamoun	Ba2	18	(Henn et al., 2011)	
Brong	Br	7 (8)	(Henn et al., 2011)	Removed 3572B (missingness > 5%).
Bulala	Bu	15	(Henn et al., 2011)	
Dogon	Do	24	(Xing et al., 2010)	
Fang	Fa	15	(Henn et al., 2011)	
Hausa	Ha	11 (12)	(Henn et al., 2011)	Removed NGHA019 (missingness > 5%).
Hema	He	13 (15)	(Henn et al., 2011)	Removed AFH7, AFH10 as PCA outliers.‡
Igbo	Ig	13 (15)	(Henn et al., 2011)	Removed NGIB007 and NGIB004 (missingness > 5%).
Kaba	Ka	17	(Henn et al., 2011)	
Kongo	Ko	9	(Henn et al., 2011)	
Luhya	Lu	23 (25)	(Henn et al., 2011)	Removed NA19027, NA19046 (not in HAP1117).†
Maasai	Ma1	21 (30)	(Henn et al., 2011)	Removed NA21528, NA21634, NA21447, NA21384, NA21382, NA21576, NA21616, NA21435, NA21405 (not in HAP1117).†
Mada	Ma2	12	(Henn et al., 2011)	
Mandenka	Ma3	22	(Henn et al., 2011)	
Nguni	Ng	9	(Xing et al., 2010)	
Pedi	Pe	10	(Xing et al., 2010)	
Sotho/Tswana	ST	8	(Xing et al., 2010)	
Xhosa	Xh	11	(Henn et al., 2011)	
Yoruba	Yo	21	(Henn et al., 2011)	Samples also in the Human Genetic Diversity Project.

Supplementary Table 2 Description of the Sub-Saharan Africa dataset, which combines data from (Xing et al., 2010) and (Henn et al., 2011). It comprises 21 ethnic groups (their names and abbreviations are given in the first and second column). The number of samples from each population are given in the third column and the source dataset in the fourth column. We excluded some samples because of issues with genotype quality or close familial relatedness. The final column indicates the excluded samples and the reason for exclusion. Notes: † The HAP1117 subset of HapMap3 excludes first- and second-degree relationships (Pemberton et al., 2010). ‡ These two Hema individuals – AFH7 and AFH10 – are classified as likely relatives and outliers in the analysis of Sub-Saharan Africa reported in (Wang et al., 2012).

S3 Supplementary Figures

List of Supplementary Figures

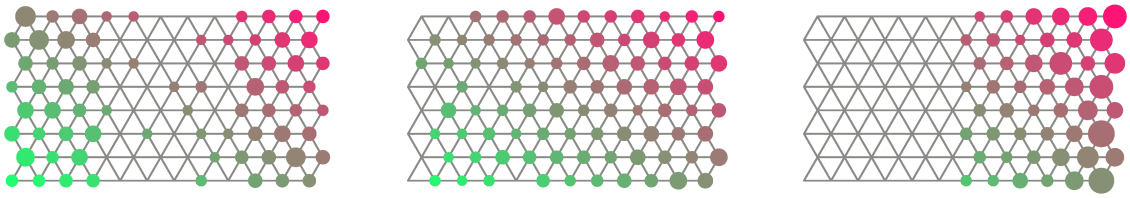

(a) Sampling configuration on a 12×8 population grid.

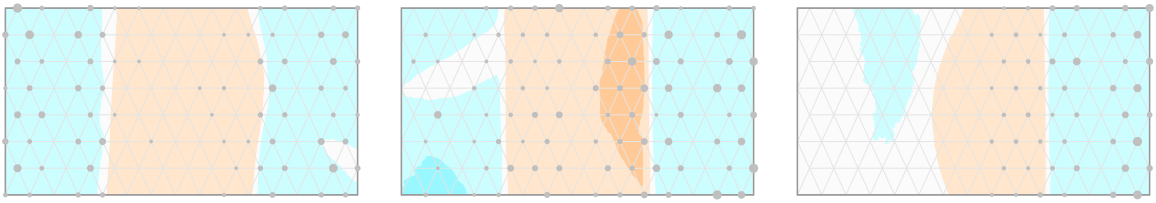

(b) Estimated effective migration rates on a 15×8 grid.

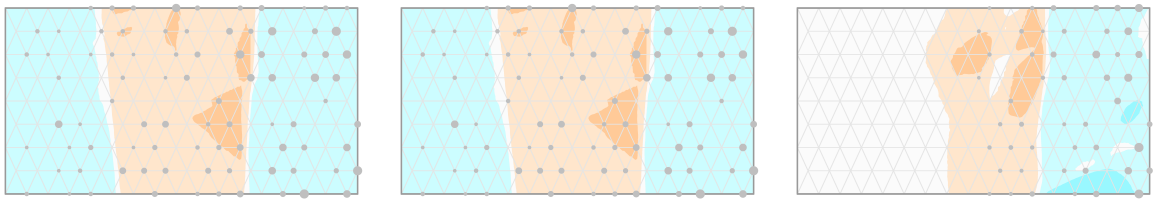

(c) Estimated effective migration rates on a 17×9 grid.

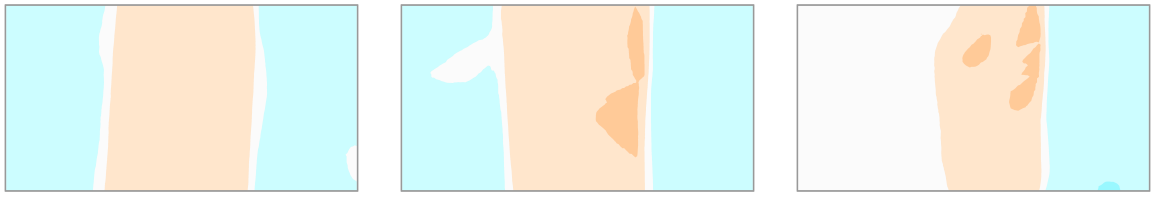

(d) Estimated effective migration rates, averaged over grids.

Supplementary Figure 1 The population grid can affect the inferred migration (and diversity) rates because (V, E) is fixed (the vertices V and the edges E are specified as input arguments to the EEMS program). For example, a very coarse grid might not allow for sufficient variation in resistance distances. Therefore, we recommend averaging the surfaces estimated with grids of different sizes – in practice this will moderate the discretization implicit in assigning the samples collected in a continuous habitat to the vertices of a discrete population graph. Here we use the barrier-to-migration simulation in Figure 2 for illustration. **(a)** The data is simulated on a 12×8 grid but we use 15×8 and 17×9 grids to estimate effective migration rates. **(b,c)** As the grid dimensions change, so do the occupied demes because samples are assigned to the closest deme in the grid. **(d)** When averaging surfaces with grids of different size, the broad features remain the same but small details can change.

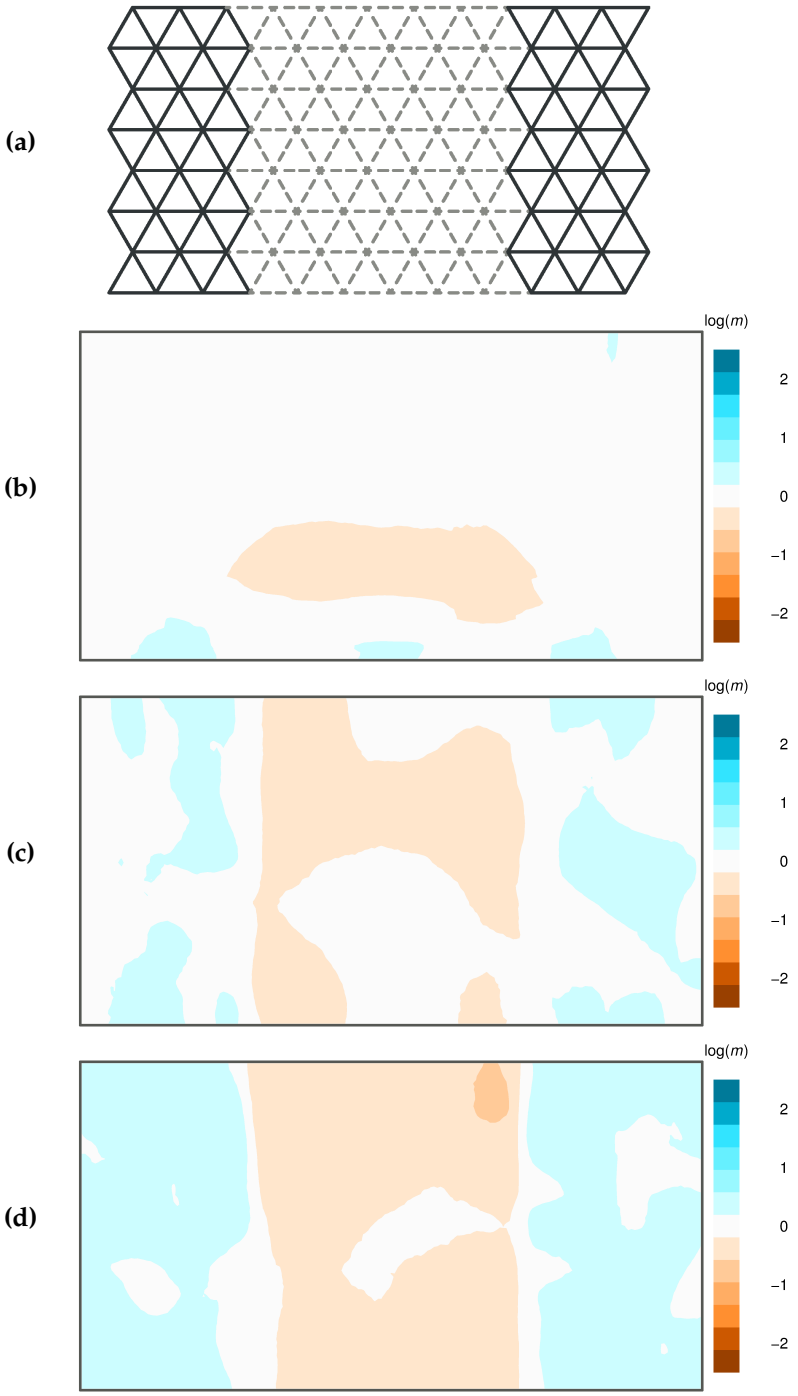

Supplementary Figure 2 A past demographic event can produce a barrier to effective migration. **(a)** An ancestral population splits into subpopulations E (east) and W (west), separated by an "effective barrier" to migration: an area where the migration rates drop simultaneously to 0 at a point of time x in the past. The further back in time the split event occurs, the more differentiated subpopulations E and W are. The split occurs at **(b)** $x = 1$; **(c)** $x = 4$; **(d)** $x = 9$ units of time in the past, which is measured in N_0 generations. Before the split, migration rates are all set to 1 (on the same coalescent scale N_0); after the split, migration rates on either side of the central region remain 1.

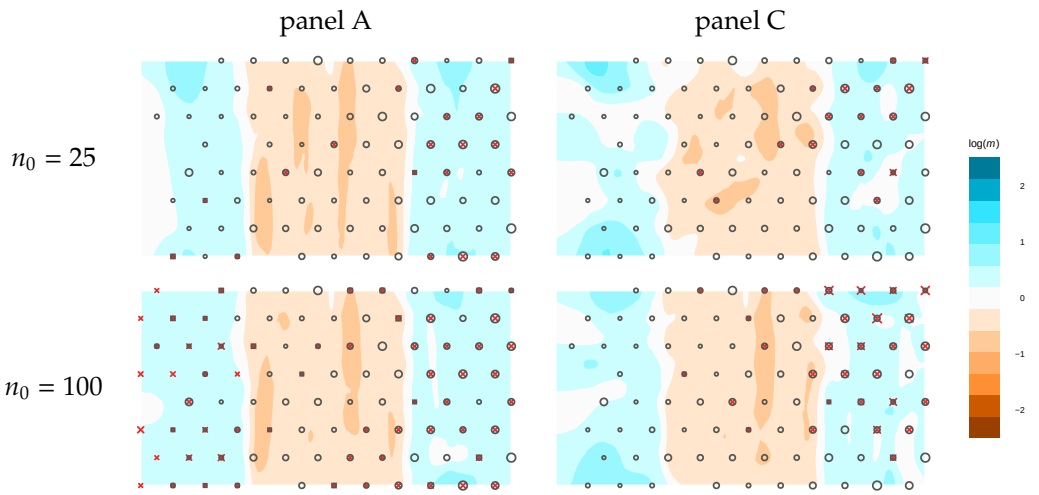

(a)

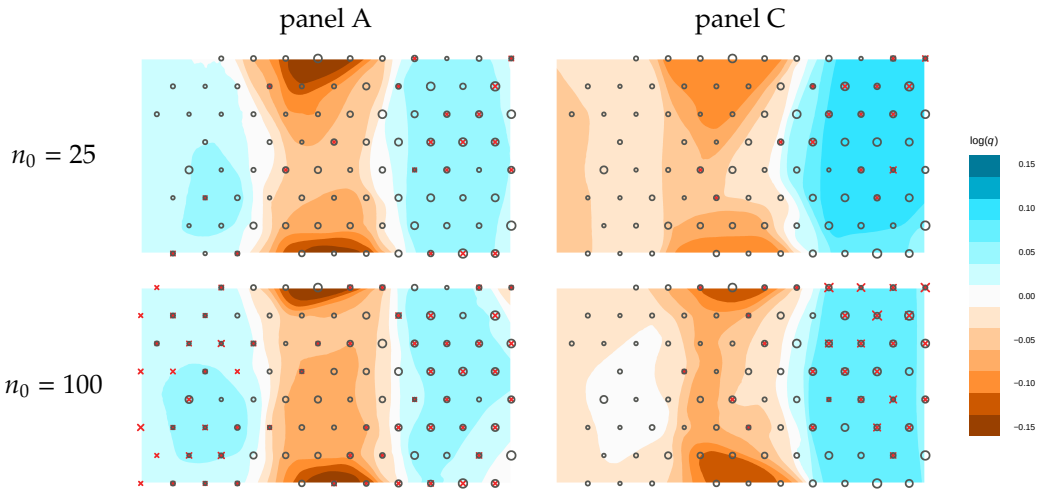

(b)

Supplementary Figure 3 The effect of geographic bias in the SNP ascertainment panel. Two samples are involved in SNP ascertainment – first a panel to discover SNPs for genotyping on a microchip and then a sample to genotype and analyze. If the discovery panel is not representative of the genetic variation in the population, then the ascertainment is biased. Here we simulate SNP ascertainment with geographic bias, under a barrier to migration scenario. We simulated $n = n_0 + n_1$ haplotypes, of which n_0 are designated discovery panel (the red crosses) and $n_1 = 300$ are designated geo-referenced sample (the black circles); there are 3000 SNPs which are polymorphic in both the discovery panel and the geo-referenced sample. SNP ascertainment is geographically biased because the discovery panel is preferentially sampled from the right than from the left of the barrier. **(a)** Effective migration rates estimates, all on the same $\log_{10}$ scale, which is indicated in the color bar on the right. **(b)** Effective diversity rates estimates, also on a common $\log_{10}$ scale. In these simulations, panel C has a stronger geographic bias than panel A and the ascertainment bias affects the diversity estimates more than the migration estimates. In panel C, the effective diversity is highest in the region where most of the discovery panel is sampled from, on the right of the barrier. Intuitively, the ascertainment process means that it is more likely to "discover" mutations that have arisen in the discovery region, hence the increase in effective diversity.

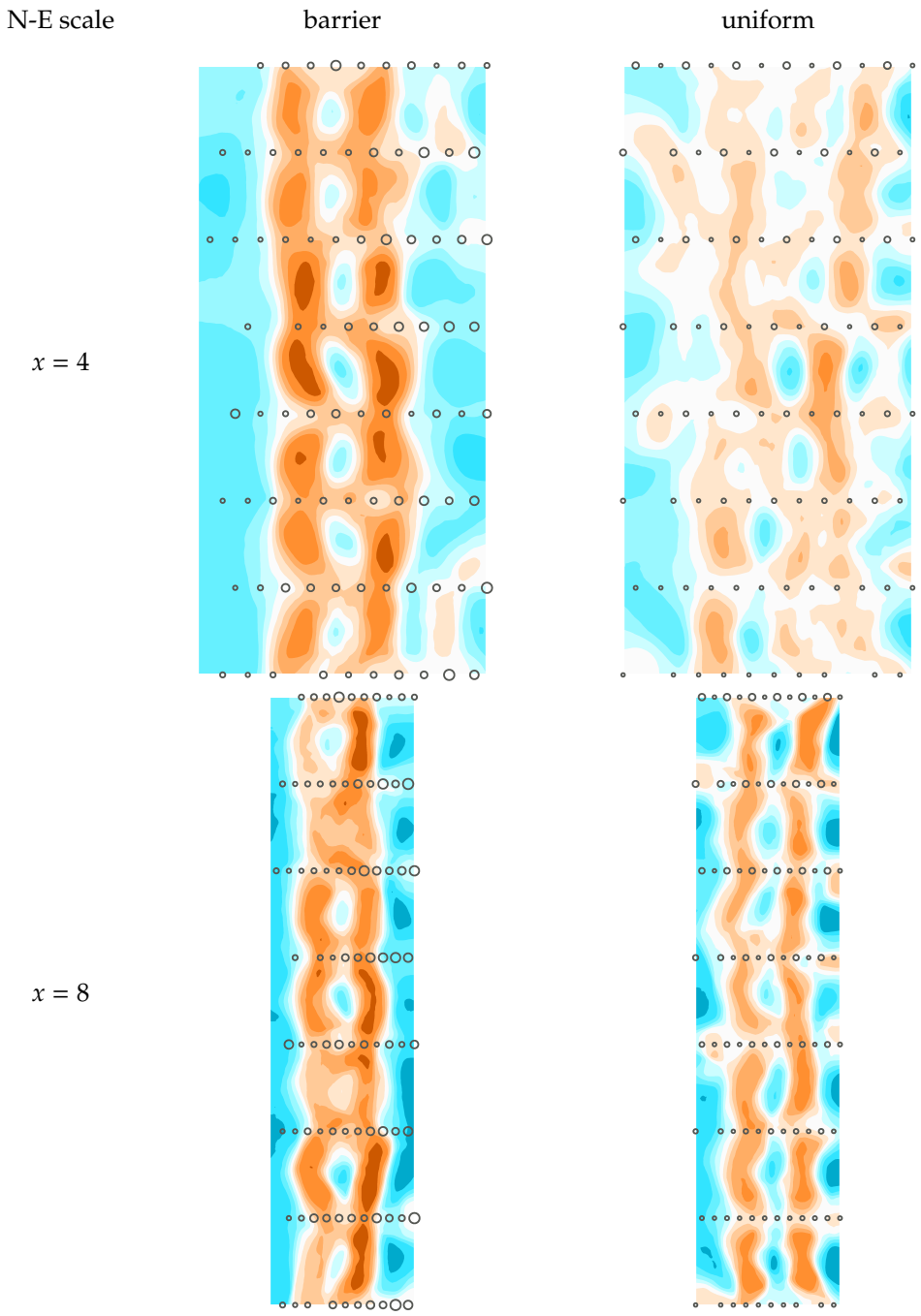

Supplementary Figure 4 The effect of migration directionality. EEMS assumes that migration is undirected and that migration rates are locally similar. Both assumptions can be violated in practice. Here we simulate migration directionality by scaling the latitude (vertical) coordinate of every sampling location by a factor x. Thus, in the same amount of time, a lineage can move x times as far in the N-S direction than in the E-W direction, i.e., N-S migration is x times as fast as E-W migration. We vary both the N-S scale factor: $x = 4$ in the top row and $x = 8$ in the bottom row, and the underlying true migration model: a barrier to migration in the left column and uniform migration in the right column. EEMS is not well suited to model migration directionality; nevertheless, it attempts to explain the spatial patterns in genetic dissimilarities by inferring N-E (vertical) barriers which effectively "slow down" migration in the E-W direction.

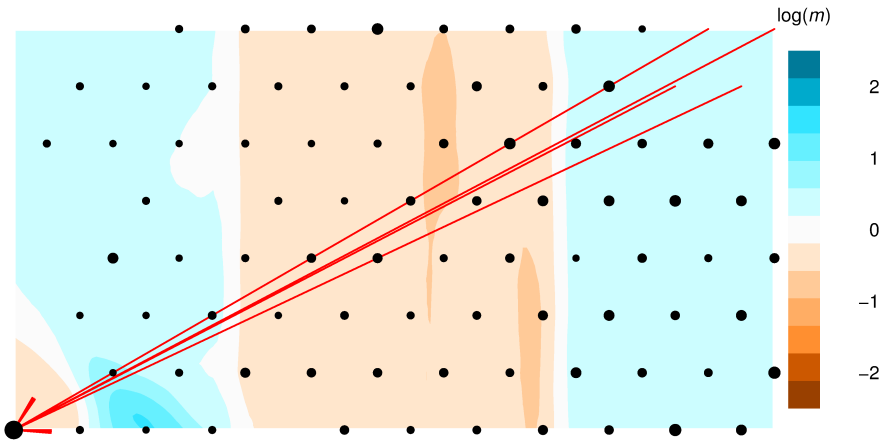

(a)

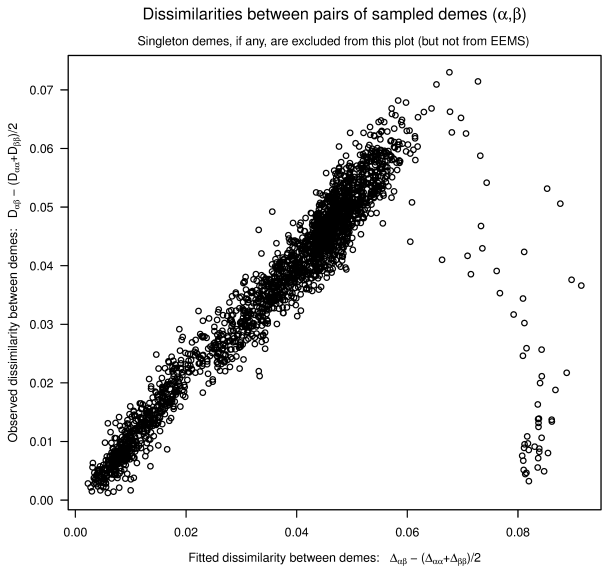

(b)

Supplementary Figure 5 Lack of fit due to recent migrants or incorrect geographic labels. In **(a)** 21 individuals from the top right corner are incorrectly assigned to the bottom left corner, as indicated by the the red arrows. The small region of low effective migration in the bottom left creates a barrier around these "migrants", capturing the fact that they are genetically distinct from other near-by individuals. Effectively, the "recipient" deme is isolated from its neighbors. However, this is not sufficient to explain the observed patterns. Hence the outliers in the diagnostic scatter plot of between-demes dissimilarities in **(b)**.

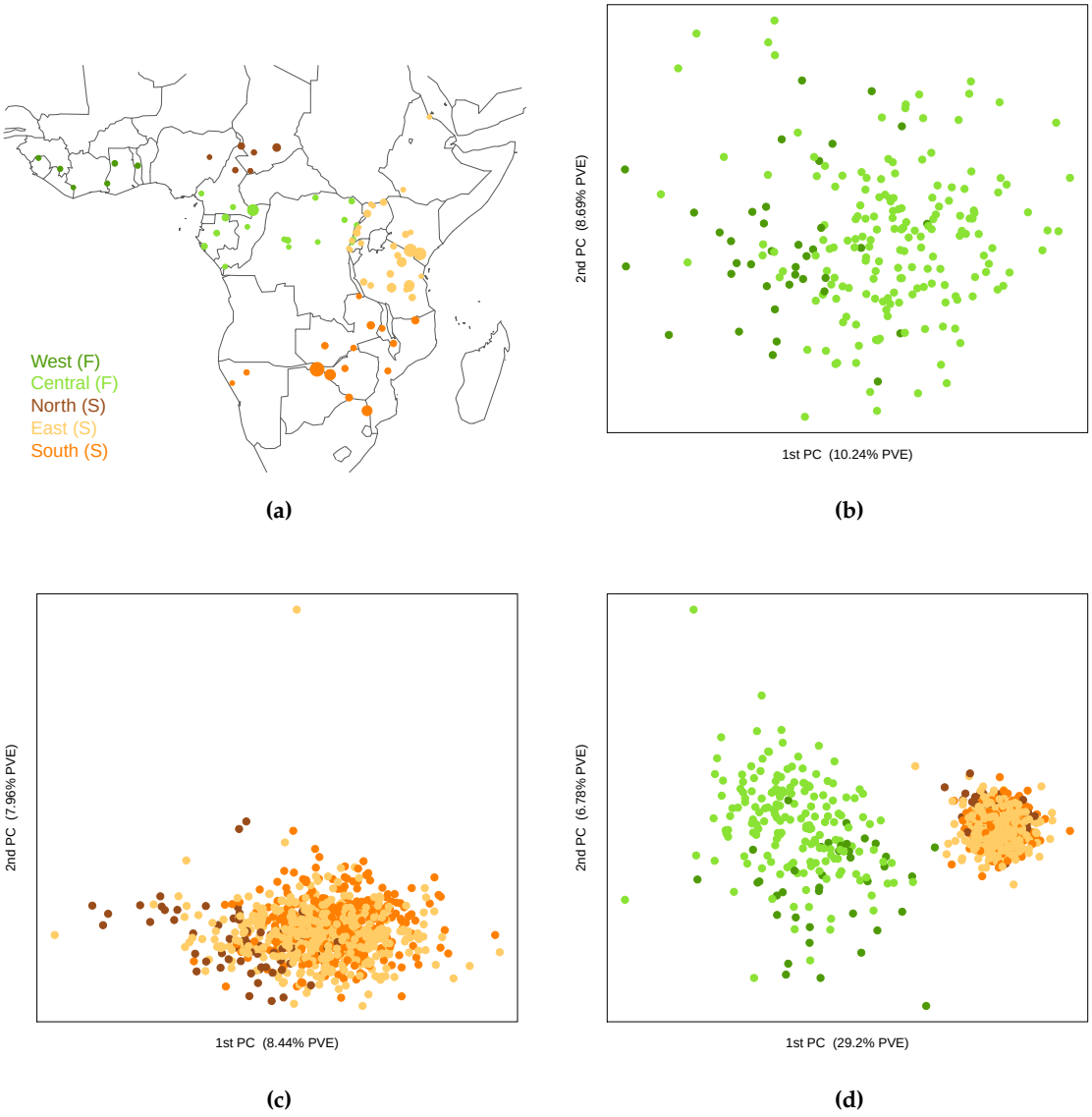

(a) **(b)** **(c)** **(d)**

Supplementary Figure 6 Principal component analysis of the African elephant data. **(a)** According to the categorization in (Wasser et al., 2004), the forest elephant subspecies inhabits the West and Central regions (in shades of green); the savanna elephant subspecies inhabits the North, East and South regions (in shades of orange). **(b-d)** First and second principal components (and the proportion of variance they explain, PVE, as a percentage). **(b)** PCA of 211 forest elephants. **(c)** PCA of 914 savanna elephants. **(d)** PCA of 1124 African elephants, both forest and savanna.

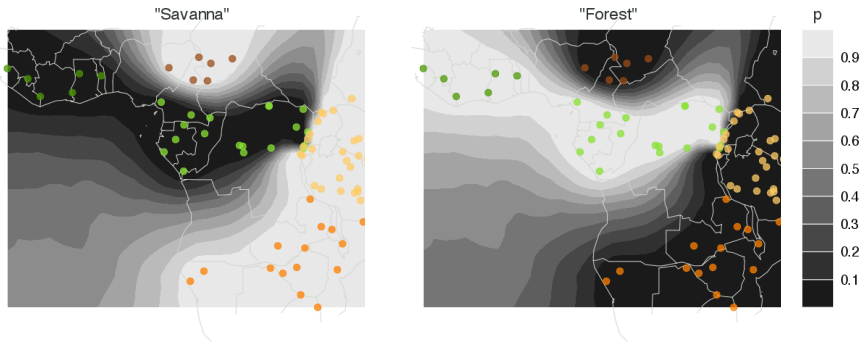

(a)

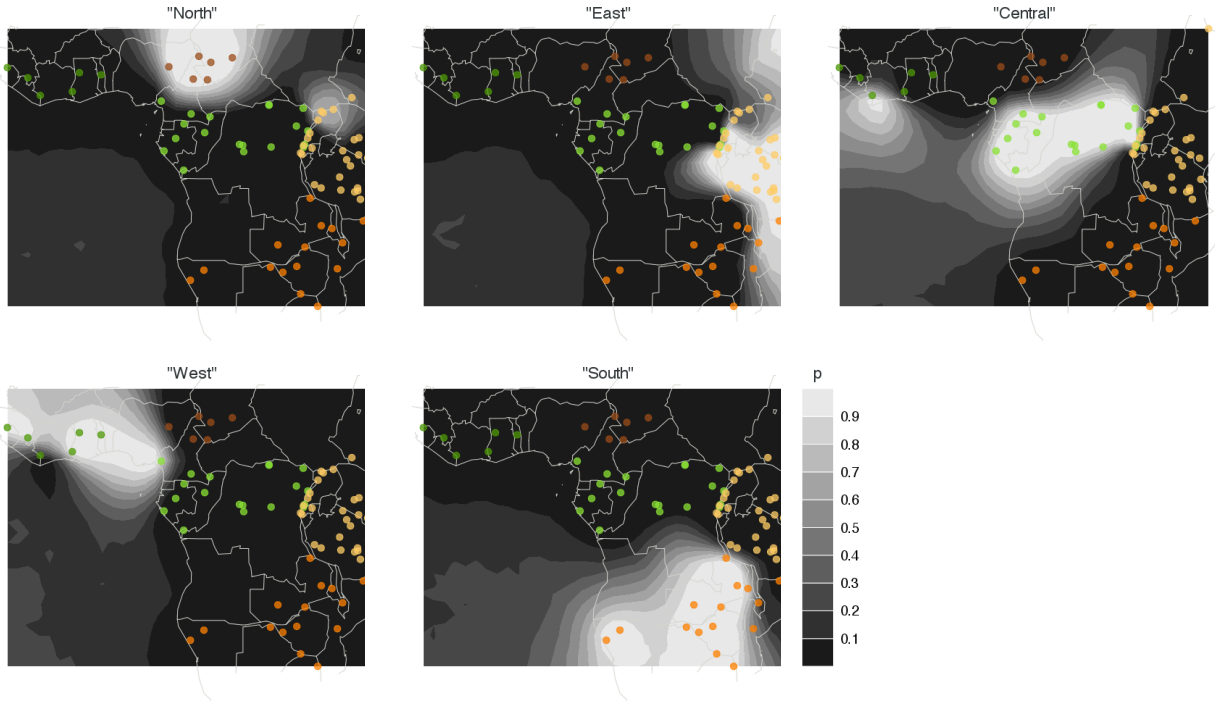

(b)

Supplementary Figure 7 GENELAND analysis of the African elephant data. GENELAND (Guillot et al., 2005) is a cluster-based method which uses a Voronoi tessellation to encourage spatially continuous clusters and find sharp boundaries between genetically differentiated groups. **(a)** Posterior probabilities for belonging to each of two inferred clusters, which correspond to the ranges of the savanna and forest subspecies. **(b)** Posterior probabilities for belonging to each of five inferred clusters, which correspond to the five biogeographic regions defined in (Wasser et al., 2004): "North", "South", "East", "West" and "Central". GENELAND successfully detects differences in allele frequencies between the two species and the five biogeographic regions. However, GENELAND does not model the relationships between the regions: the five clusters in (b) are as distinct from each other as the two clusters in (a), even though the "West" and "Central" clusters are inhabited by forest elephants while the "North", "East" and "South" clusters – by savanna elephants.

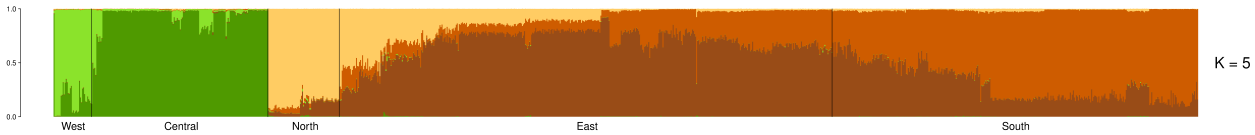

(a)

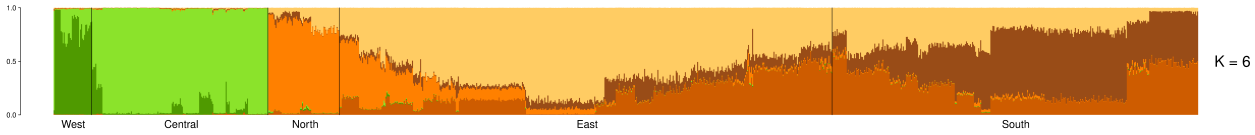

(b)

Supplementary Figure 8 STRUCTURE analysis of the African elephant data. **(a)** Membership proportions for belonging to five inferred clusters. **(b)** Membership proportions for belonging to six inferred clusters. Individuals are ordered by sampling location and the five biogepgraphic regions and separated by black vertical lines; the ancestral populations of forest and savanna elephants are colored in green and brown hues, respectively. Compared to GENELAND (Guillot et al., 2005), STRUCTURE (Pritchard et al., 2000) with a sampling location prior (Hubisz et al., 2009) provides intuition for the relationship between the five biogeographic regions. STRUCTURE clearly detects the difference between forest elephants (West and Central regions) and savanna elephants (North, East and South regions) as they fall into different clusters. Furthermore, STRUCTURE shows some evidence for isolation by distance, particularly in savanna elephants, as most of these individuals are represented as weighted mixtures of ancestral clusters that do not correspond to distinct geographic areas.

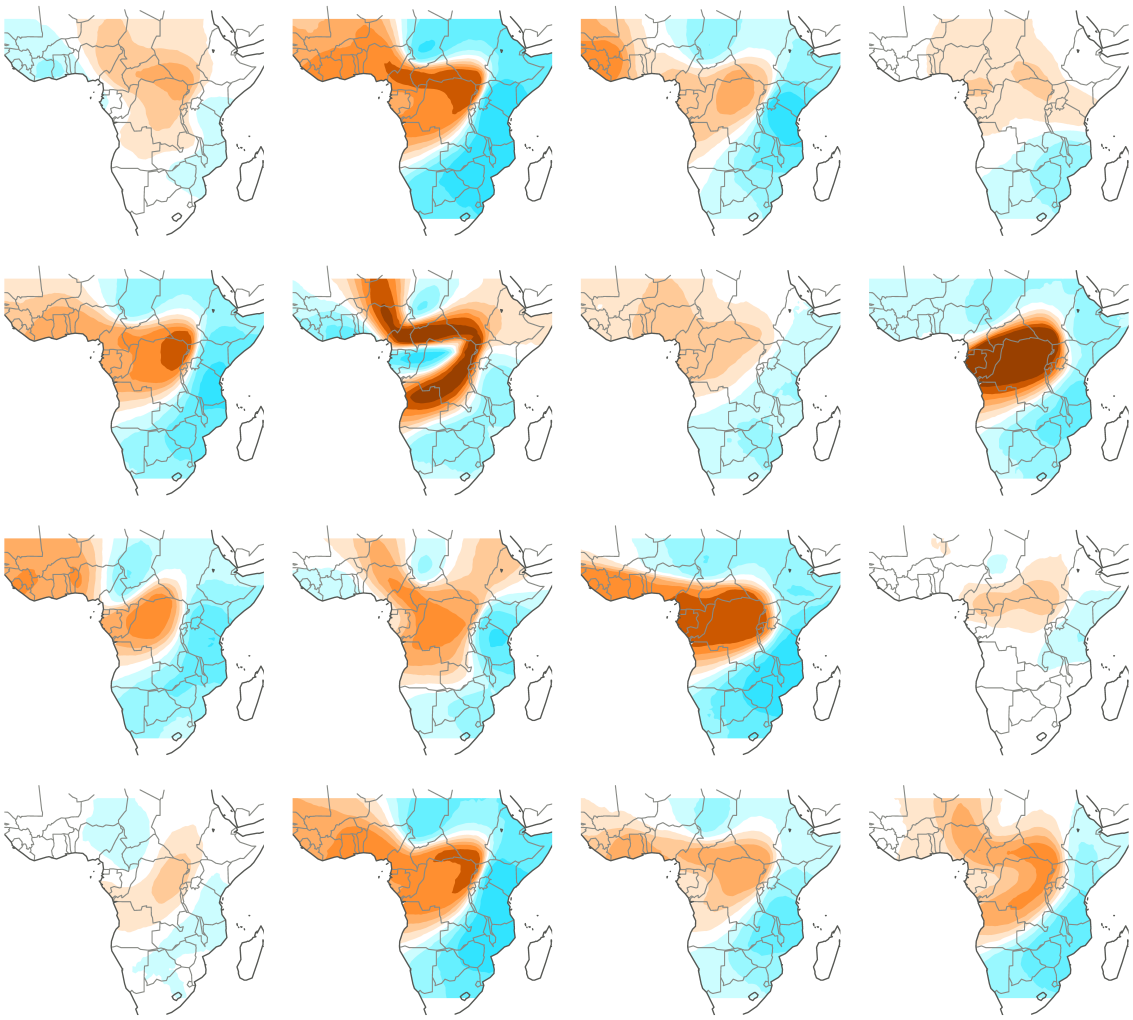

Supplementary Figure 9 Effective migration rates for the African elephant at sixteen microsatellite loci. The loci are highly polymorphic and therefore informative for the sample genealogy at each site: every mutation on the genealogy contains information about the branch lengths in the tree (since longer branches are more likely to carry a mutation, if the mutation rate is constant in time). The sixth locus is extremely informative, presumably because it has the highest mutation rate, and it successfully captures the strong effective barrier to migration between the habitat ranges of forest and savanna elephants.

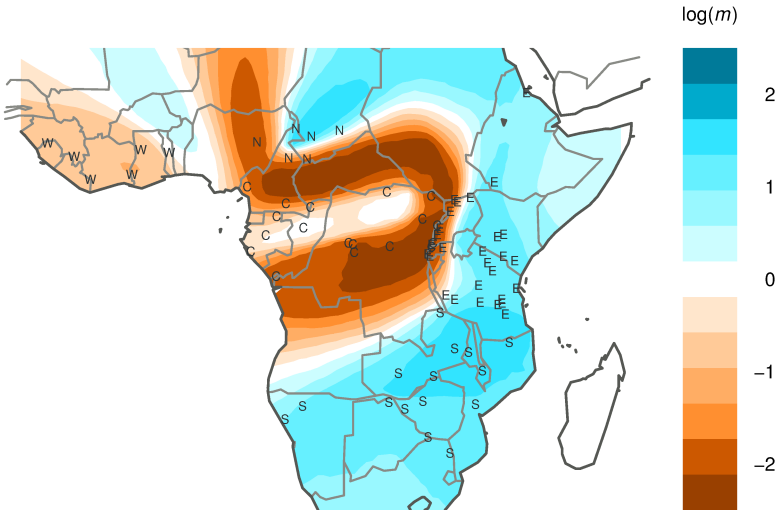

(a)

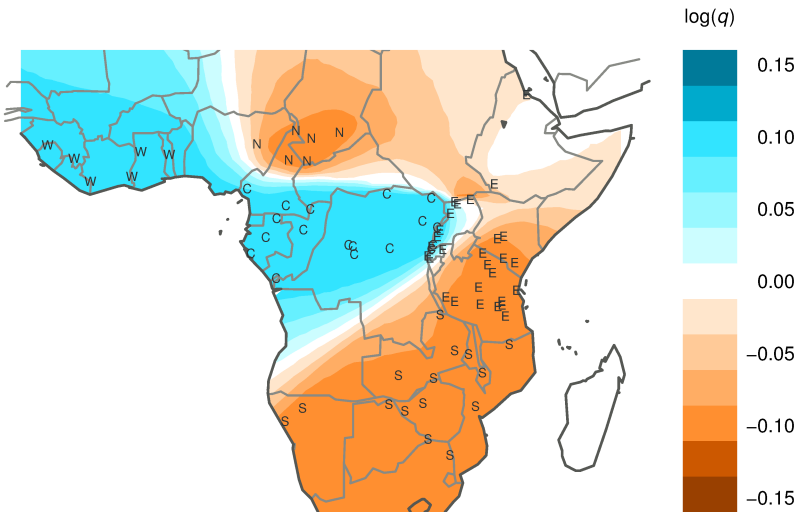

(b)

Supplementary Figure 10 Further EEMS analysis of the population structure of the African elephant data from (Wasser et al., 2015). According to the categorization in (Wasser et al., 2004), forest elephants come from two regions: West (W) and Central (C); savanna elephants come from three regions: North (N), East (E) and South (S). **(a)** Estimated effective migration surface, after excluding the most variable locus – the sixth locus in **Supplementary Figure 9**. It separates the two subspecies of African elephnts, forest and savanna. **(b)** Estimated effective diversity rates using all sixteen loci. Forest elephants have higher effective diversity than savanna elephants. This is consistent with previous analysis which indicates that forest elephants have higher average heterozygosity (Comstock et al., 2002).

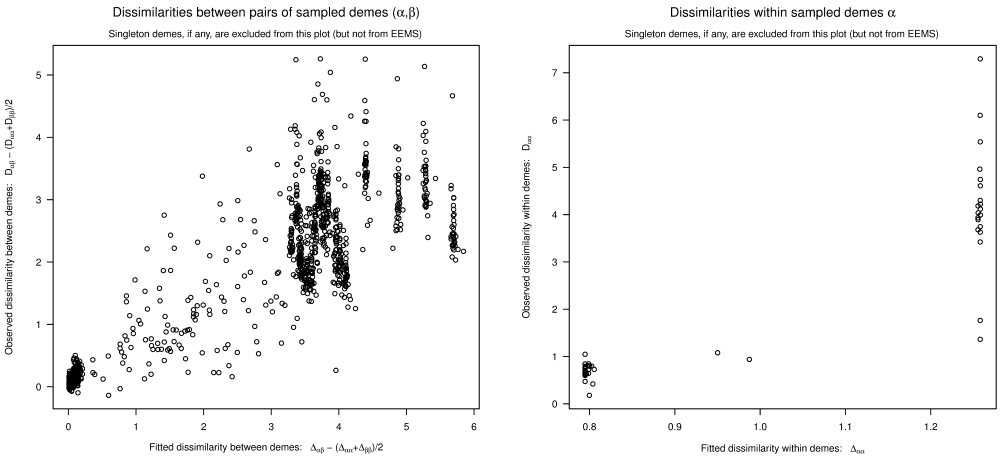

(a) **(b)**

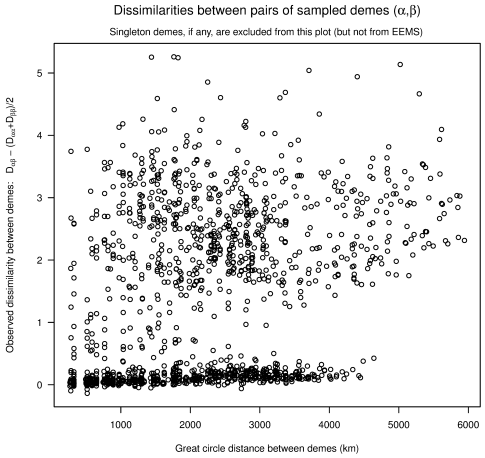

(c)

Supplementary Figure 11 Observed vs fitted genetic dissimilarities, between and within demes, for the African elephants. The observed genetic dissimilarities between individuals, D_{ij}, are averaged so that $D_{\alpha\beta} = \frac{1}{n_{\alpha\beta}} \sum_{\delta(i)=\alpha,\delta(j)=\beta,i\neq j} D_{ij}$ where $n_{\alpha\beta}$ is the number of pairs (i, j) such that $\delta(i) = \alpha$, $\delta(j) = \beta$, i.e., sample i is assigned to deme α, sample j is assigned to deme β, and i, j are distinct individuals. Singleton demes (those with a single sample) are excluded from both scatter plots. **(a)** Dissimilarities between demes. The fitted values $B_{\alpha\beta} = \Delta_{\alpha\beta} - (\Delta_{\alpha\alpha} + \Delta_{\beta\beta})/2$ comprise the between-demes component of genetic dissimilarity, B, which is modeled by the effective migration rates m as in equation (S14). **(b)** Dissimilarities within demes. The fitted values $W_\alpha = \Delta_{\alpha\alpha}$ comprise the within-demes component of genetic dissimilarity, W, which is modeled by the effective diversity rates q as in equation (S13). If the EEMS model fits the data well, we expect a strong linear relationship between the observed and fitted values in both scatter plots. **(c)** Genetic dissimilarities against geographic distances between demes. If isolation by distance (IBD) explains the spatial patterns in the data well, we expect a strong linear relationship between genetic dissimilarity and geographic distance. The African elephants violate exact IBD because forest and savanna elephants are strongly differentiated even though their habitats are side by side, particularly in the hybrid zone in Central Africa (the Democratic Republic of the Congo).

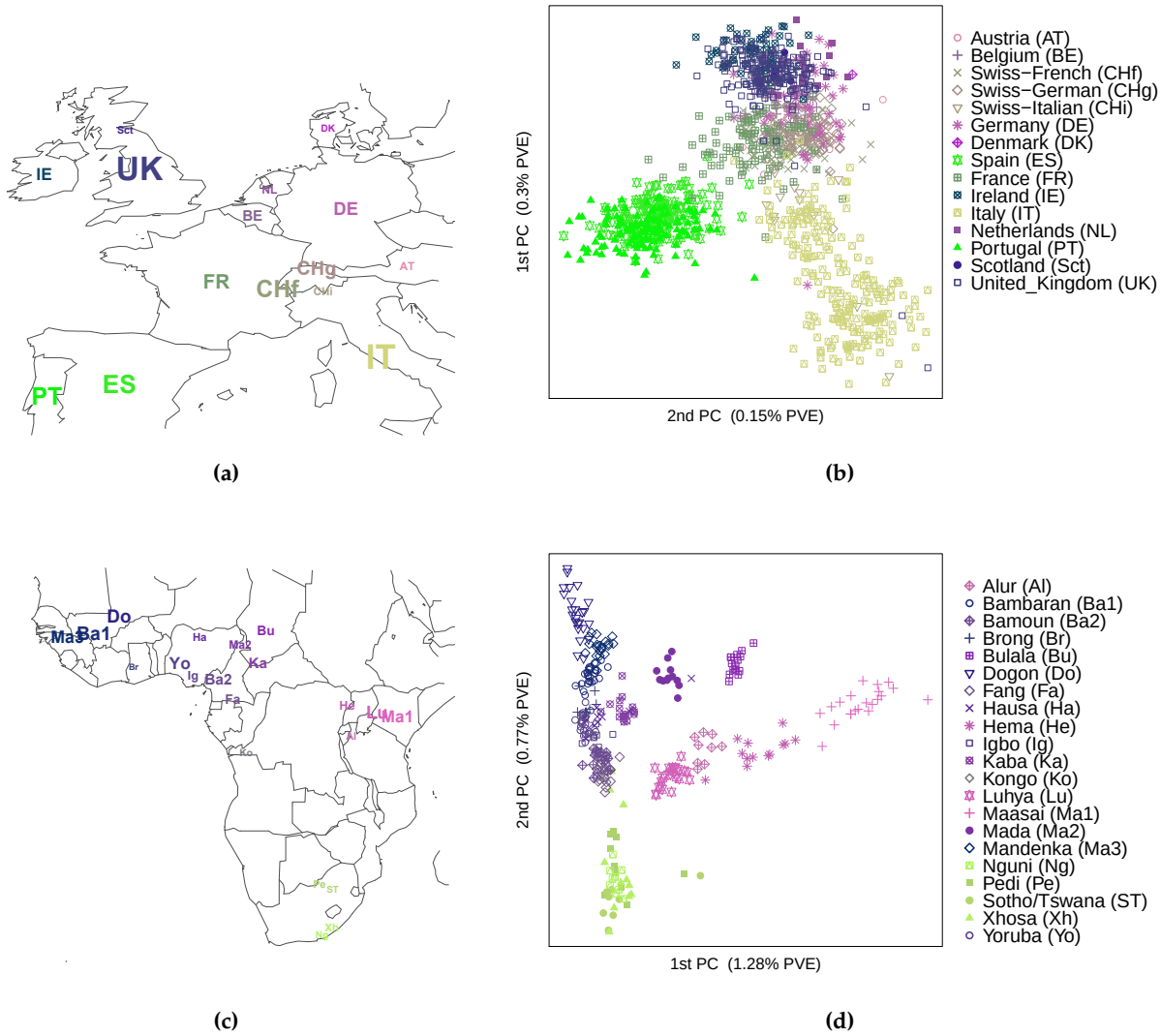

Supplementary Figure 12 Principal component analysis of humans in Western Europe and Sub-Saharan Africa. **(a)** We analyze 1201 individuals from 15 Western European populations. The data is part of the POPRES (Population Reference Sample) project (Nelson et al., 2008). The populations and their abbreviations are given in the legend on the right. The sampling is uneven and the size of the symbol indicates the relative number of individuals from each population. Colors are assigned according to latitude and longitude. **(b)** The first and second principle components are strongly correlated with latitude and longitude, as reported in (Novembre et al., 2008), and explain 0.3% and 0.15% of the observed genetic variation. **(c)** We analyze 314 individuals from 21 Sub-Saharan ethnic groups. The data is a compilation of two published SNP array datasets described in (Xing et al., 2010) and (Henn et al., 2011). Again, the symbols and colors are assigned according to geographic location and sample size. **(d)** The first and second principle components are strongly correlated with longitude and latitude, as reported in (Wang et al., 2012), and explain 1.3% and 0.8% of the observed genetic variation.

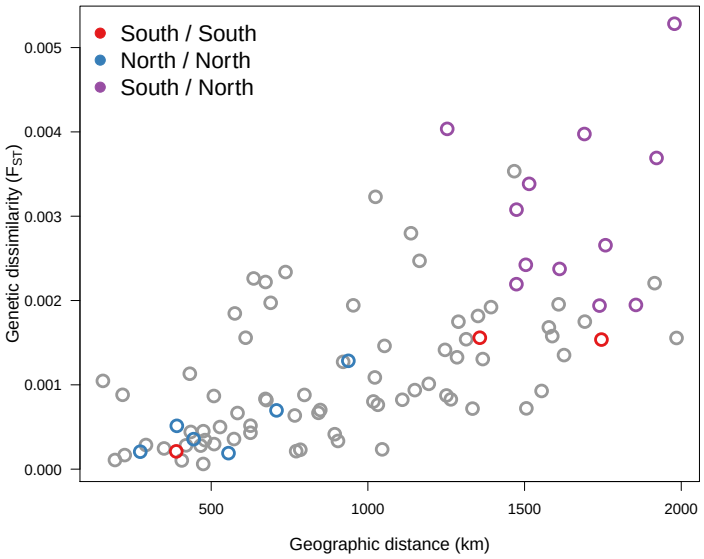

(a)

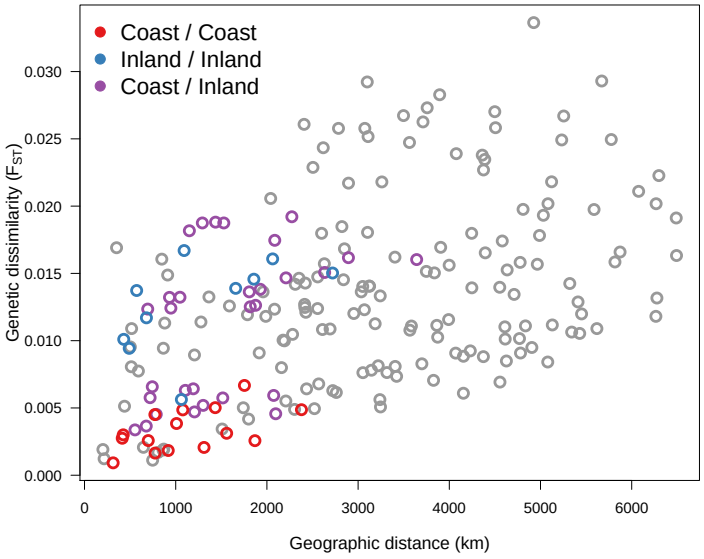

(b)

Supplementary Figure 13 Genetic dissimilarity (F_{ST}) as a function of geographic (great circle) distance, for pairs of human populations in Western Europe and Sub-Saharan Africa. On both continents, genetic differentiation increases with distance and this suggests that spatial variation is consistent with isolation by distance. The colors are chosen to emphasize comparisons between two groups of populations. **(a)** In Western Europe, the "south" group consists of Portugal (PT), Spain (ES), Italy (IT); the "north" group consists of Ireland (IE), Scotland (Sct), United Kingdom (UK), Holland (NL). Comparisons within the "south" and "north" groups are colored red and blue, respectively; comparisons between the two groups are colored purple. There is greater similarity within each group than between the groups. **(b)** In Sub-Saharan Africa, the "coast" group consists of Brong (Br), Yoruba (Yo), Igbo (Ig), Bamoun (Ba2), Fang (Fa), Kongo (Ko); the "inland" group consists of Hausa (Ha), Mada (Ma2), Bulala (Bu), Kaba (Ka), Hema (He). Coastal populations are more similar genetically than inland populations, even though some coastal populations are further apart.

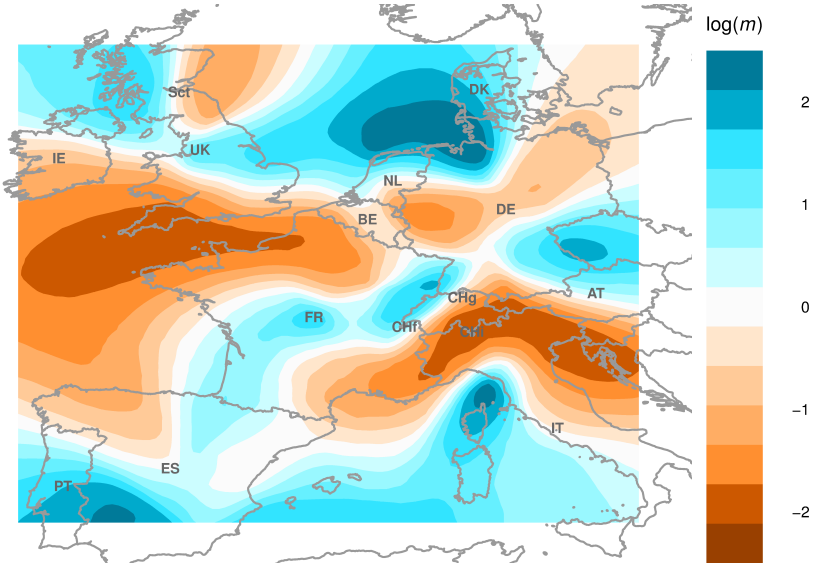

(a)

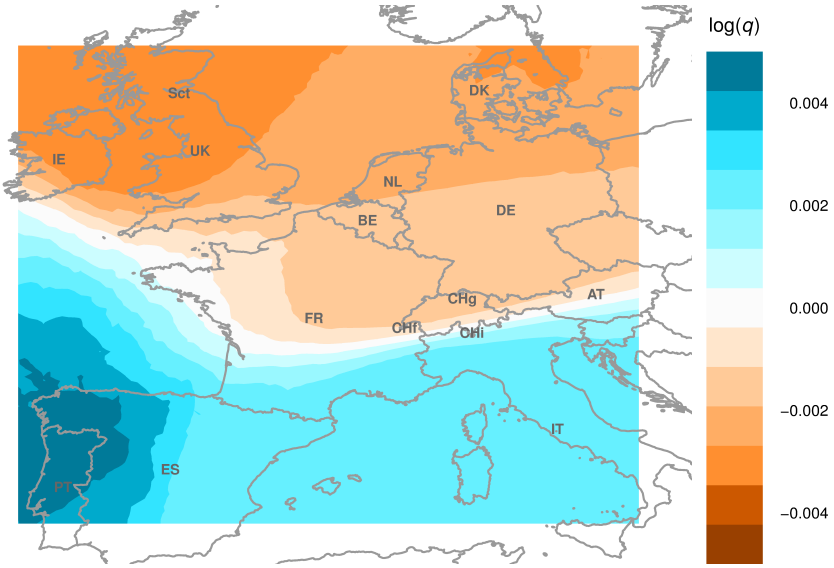

(b)

Supplementary Figure 14 EEMS analysis of the spatial structure of genetic variation in Western European, using data from the POPRES project (Nelson et al., 2008). EEMS estimates the effective diversity rates within demes, jointly with the effective migration rates between connected demes. The fitted diversity rates can be interpolated across the habitat to produce an "estimated effective diversity surface", which is complementary to the "estimated effective migration surface". **(a)** Effective migration rates. This contour plot highlights effective barriers to migration in the north-south direction. **(b)** Effective diversity rates. This contour plot highlights the previously noted north-south gradient in human genetic diversity in Europe (Lao et al., 2008; Auton et al., 2009).

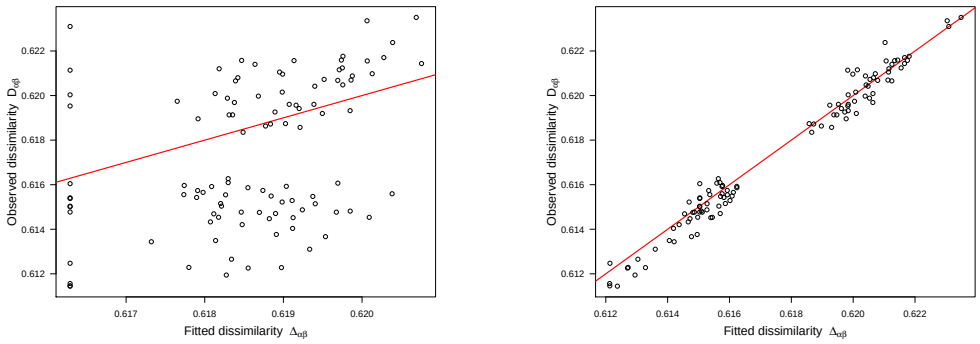

(a) **(b)**

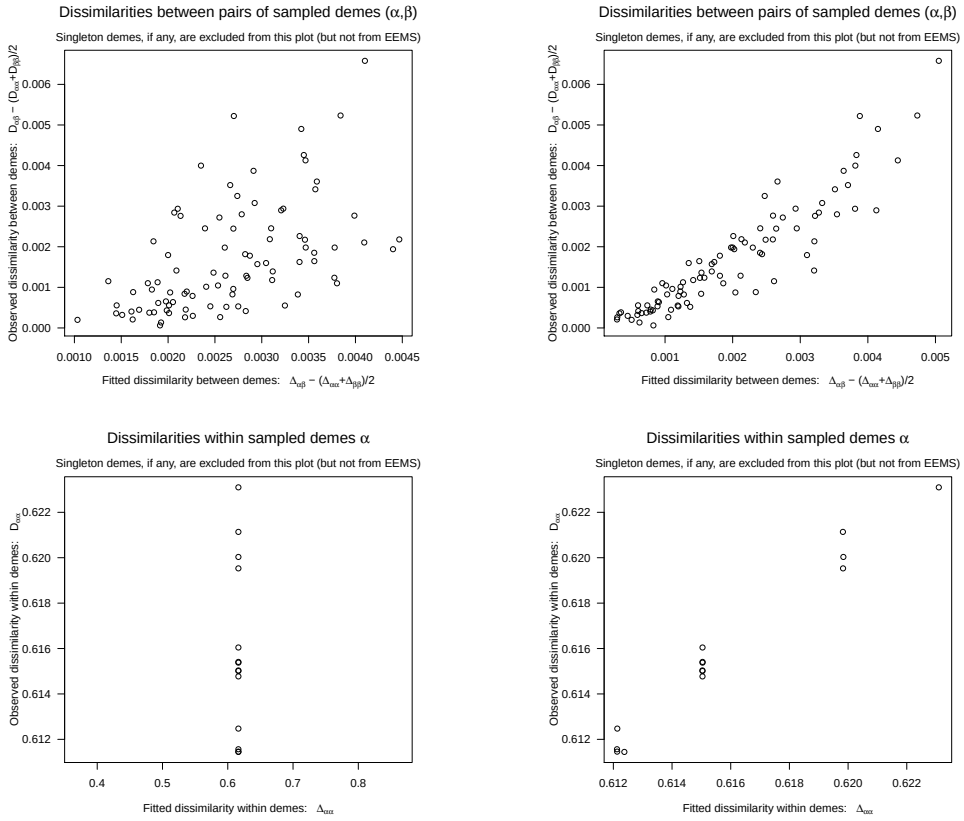

(c) **(d)**

Supplementary Figure 15 Observed versus fitted dissimilarities between the 14 Western European populations in **Supplementary Table 1**, excluding Denmark (DK), with a single sampled individual. Since in EEMS the fitted genetic distances predict the observed genetic differences, the coefficient of determination, r^2, between the fitted and observed values indicates the goodness-of-fit, for a specific population grid. (Here the grid is 19×15.) **(a)** Dissimilarities are modeled under the assumption of uniform migration, a setting which simulates exact isolation by distance; $r^2 = 0.142$ for IBD. **(b)** Dissimilarities are modeled with EEMS, which estimates both the effective migration rates and the effective diversity rates, assuming equilibrium in time; $r^2 = 0.978$ for EEMS. Genetic dissimilarities can be further decomposed into a between-demes and a within-demes component, and the fitted and observed values for the two components plotted separately, as in **(c,d)** for IBD and EEMS, respectively. This pair of diagnostic plots are automatically generated by the EEMS software, to help assess the EEMS model fit.

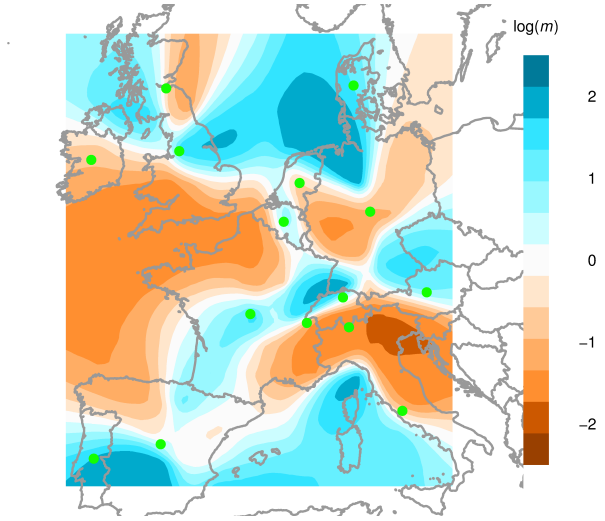

(a)

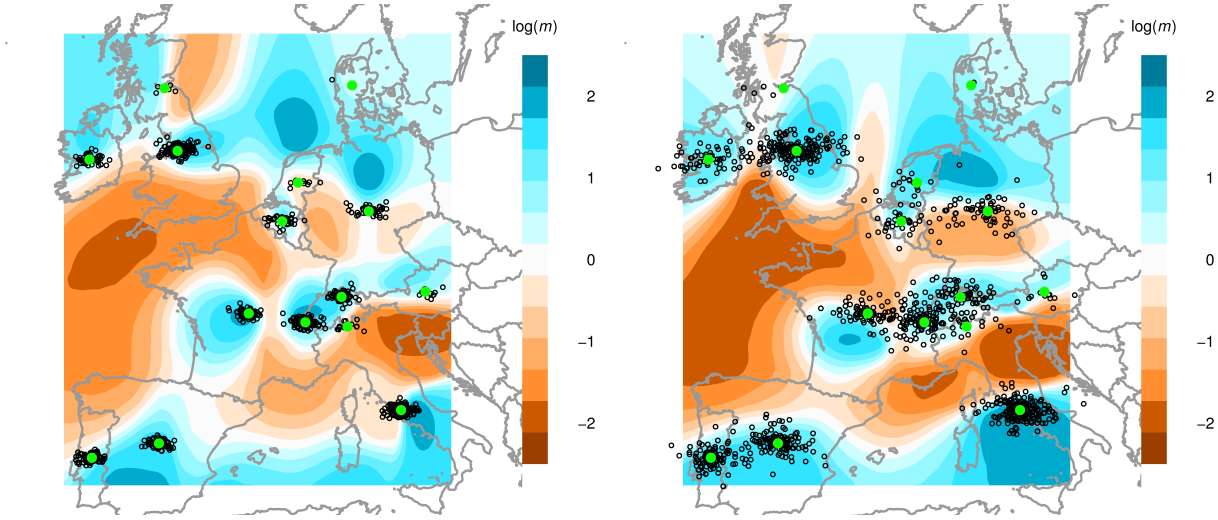

(b) (c)

Supplementary Figure 16 Robustness of estimated effective migration rates to unbiased location uncertainty, using data from the POPRES project (Nelson et al., 2008). In this dataset geographic information is imprecise: except for Switzerland, nationals from the same country are assigned to the central point of its area. Swiss individuals are categorized into Swiss-German, Swiss-French and Swiss-Italian, and assigned to three different locations within Switzerland. **(a)** Effective migration surface with the original assigned coordinates, indicated in green. **(b,c)** Effective migration surface after adding an unbiased random error to the assigned location of each individual. The "jittered" coordinates are in black, the original coordinates in green. The effective migration surface is robust to small unbiased location errors, except in sparsely sampled geographic regions. In this case, the effective migration estimates vary the most in the top right corner where there is a single individual from Denmark.

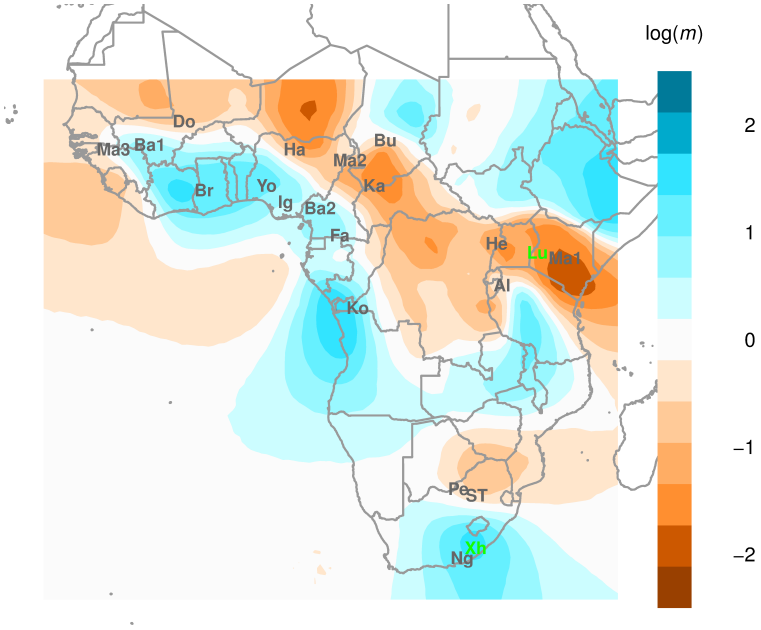

(a)

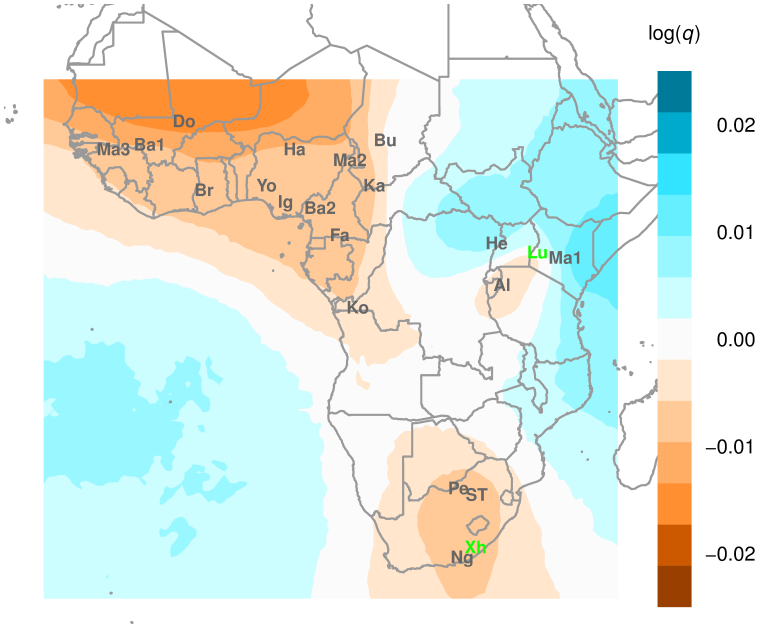

(b)

Supplementary Figure 17 EEMS analysis of 314 individuals from 21 Sub-Saharan African ethnic groups: Alur (Al), Bambaran (Ba1), Bamoun (Ba2), Brong (Br), Bulala (Bu), Dogon (Do), Fang (Fa), Hausa (Ha), Hema (He), Igbo (Ig), Kaba (Ka), Kongo (Ko), Luhya (Lu), Maasai (Ma1), Mada (Ma2), Mandenka (Ma3), Nguni (Ng), Pedi (Pe), Sotho/Tswana (ST), Xhosa (Xh), Yoruba (Yo). The Luhya and Xhosa populations, highlighted in green, are recent geographic migrants (Henn et al., 2011). We remove these two populations and re-analyze the Sub-Saharan data in **Supplementary Figure 18**. **(a)** Effective migration rates. This contour plot emphasizes the higher effective migration along the Atlantic coast. **(b)** Effective diversity rates. This contour plot emphasizes the higher effective diversity in East Africa than in South or West Africa.

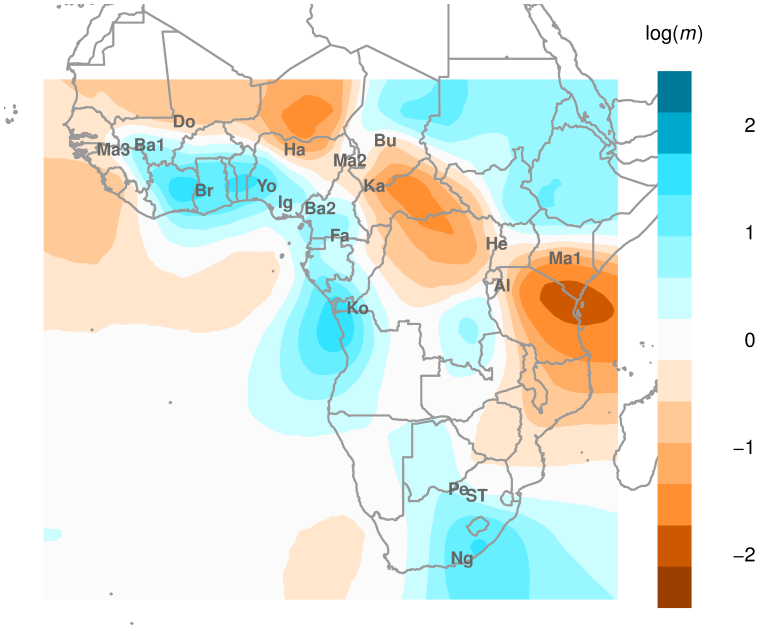

(a)

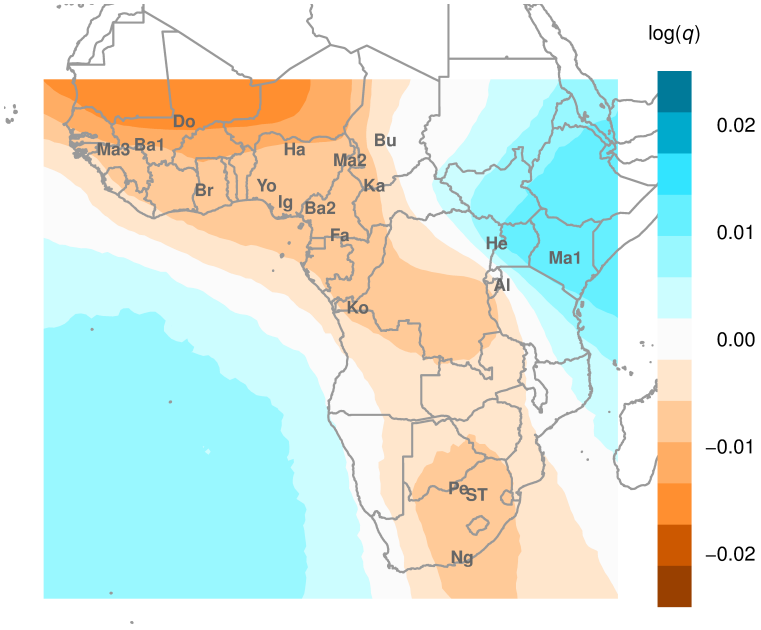

(b)

Supplementary Figure 18 EEMS analysis of the spatial structure in 19 Sub-Saharan African populations, after excluding the Luhya (Lu) and the Xhosa (Xh), two Bantu speaking populations considered recent geographic migrants in (Henn et al., 2011). EEMS approximates a spatial demographic model which evolves under equilibrium in time and recent migration deviates from this assumption. The other Bantu speaking populations are Pedi (Pe), Sotho/Tswana (ST) and Nguni (Ng) in the south and Fang (Fa) and Kongo (Ko) in the west. **(a)** Effective migration rates. **(b)** Effective diversity rates.

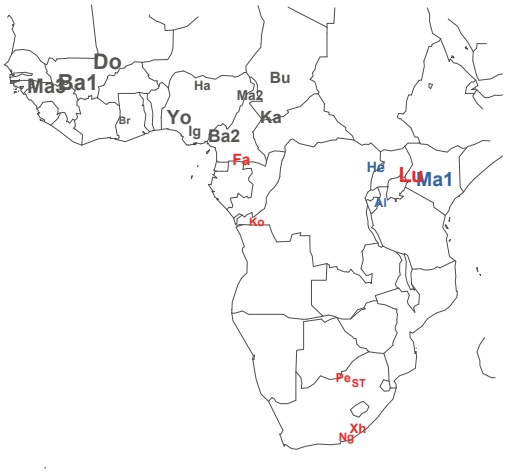

(a)

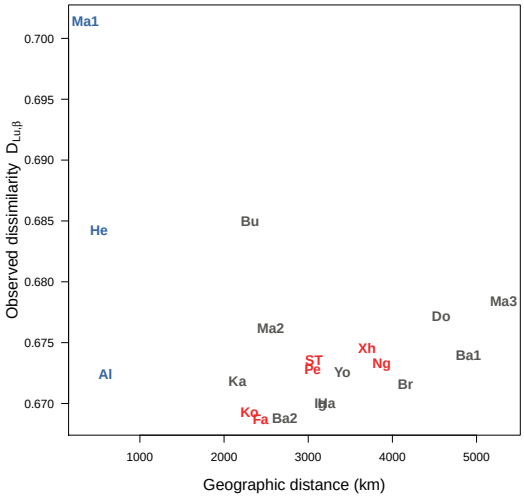

(b)

Supplementary Figure 19 Geographic distances and genetic dissimilarities between a recent migrant population (the Luhya, who speak a Bantu language) and 20 other ethnic groups in Sub-Saharan Africa. **(a)** The populations highlighted in red speak Bantu languages, the populations highlighted in blue speak Nilotic languages. The population names are given in **Supplementary Table 2**. **(b)** Observed genetic dissimilarity vs geographic distance between one Bantu speaking population – the Luhya (Lu) in the east – and each of the other 20 ethnic groups in the Sub-Saharan Africa dataset. The Luhya are geographically close to the other ethnic groups in the east but are genetically differentiated from the Hema (He) and the Maasai (Ma1). The Luhya are recent geographic migrants (Henn et al., 2011), which could explain the difference between the EEMS in **Supplementary Figure 17**, which includes the Luhya, and the EEMS in **Supplementary Figure 18**, which excludes the Luhya.

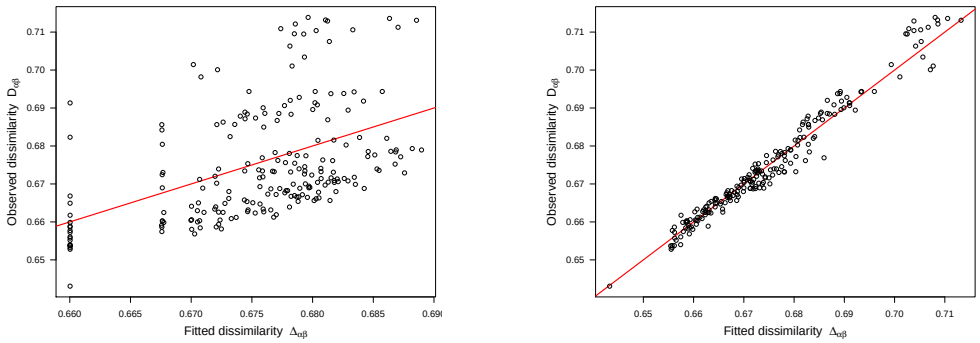

(a) **(b)**

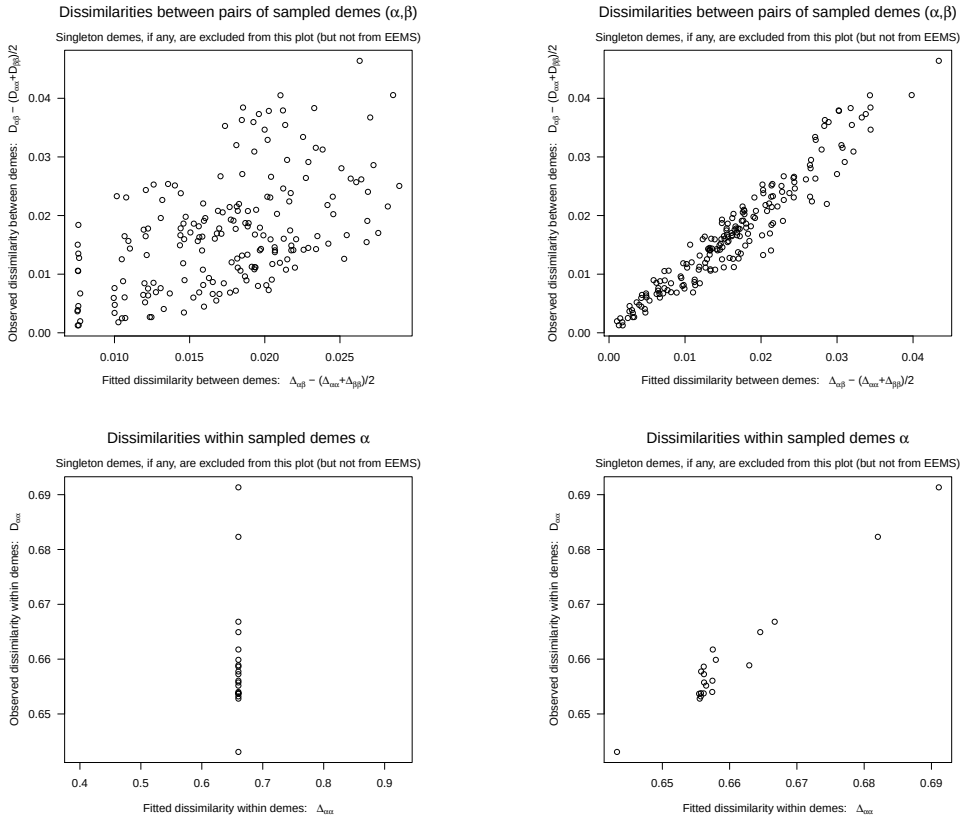

(c) **(d)**

Supplementary Figure 20 Observed versus fitted dissimilarities between the 21 Sub-Saharan ethinic groups in **Supplementary Table 2**. Since in EEMS the fitted genetic distances predict the observed genetic differences, the coefficient of determination, r^2, between the fitted and observed values indicates the goodness-of-fit, for a specific population grid. (Here the grid is 19×17.) **(a)** Dissimilarities are modeled under the assumption of uniform migration, a setting which simulates exact isolation by distance; $r^2 = 0.164$ for IBD. **(b)** Dissimilarities are modeled with EEMS, which estimates both the effective migration rates and the effective diversity rates, assuming equilibrium in time; $r^2 = 0.914$ for EEMS. Genetic dissimilarities can be further decomposed into a between-demes and a within-demes component, and the fitted and observed values for the two components plotted separately, as in **(c,d)** for IBD and EEMS, respectively. This pair of diagnostic plots are automatically generated by the EEMS software, to help assess the EEMS model fit.

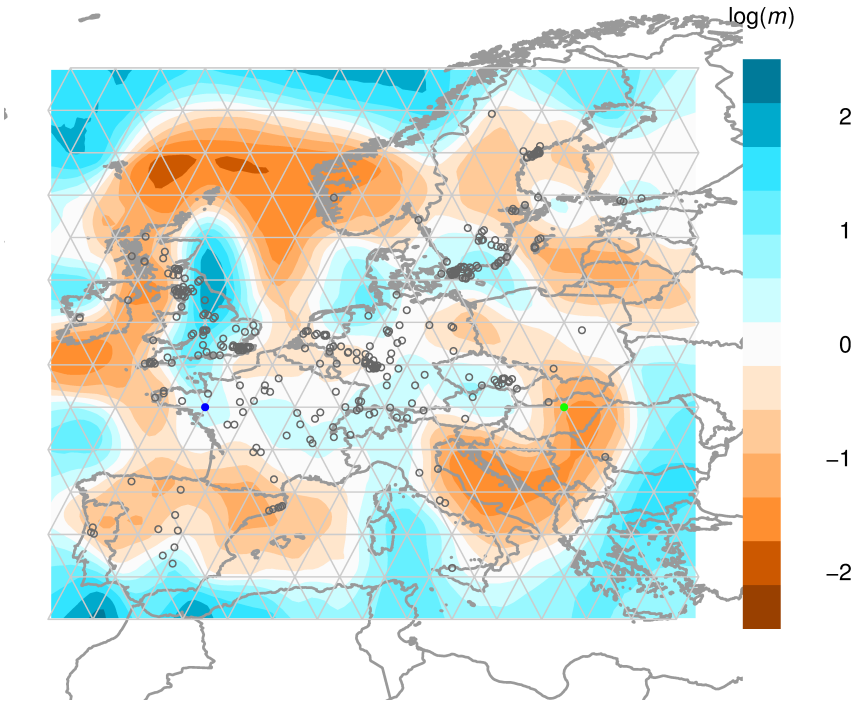

(a)

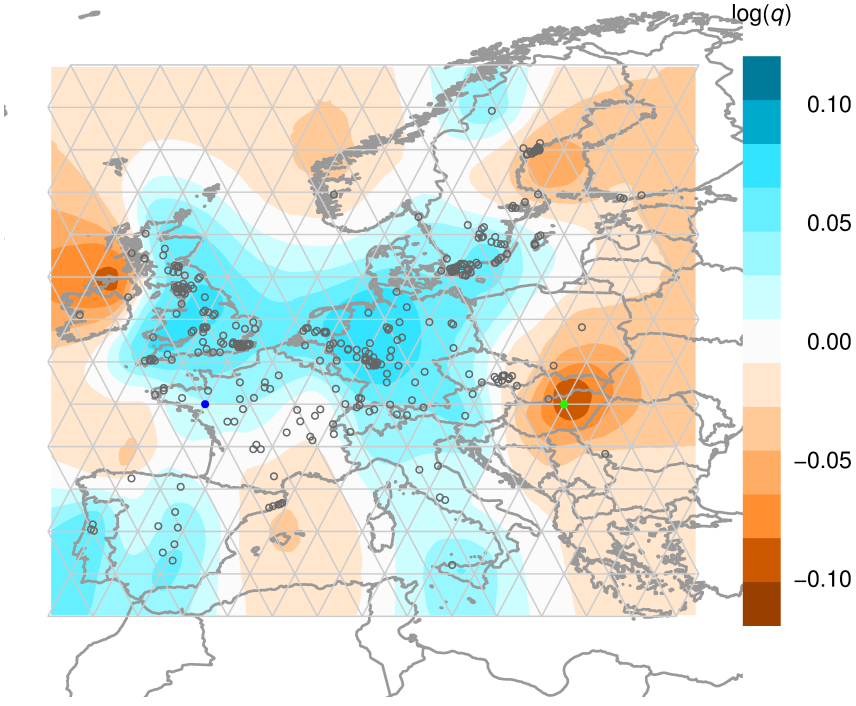

(b)

Supplementary Figure 21 EEMS analysis of 980 *Arabidopsis thaliana* accessions collected in Europe; georeferenced data from the RegMap project (Horton et al., 2012). **(a)** Effective migration surface. There is relatively little variation in migration rates across continental Europe (France, Germany, Central Europe), as expected under isolation by distance (Platt et al., 2010). **(b)** Effective diversity surface. Diversity is highest in Germany and Central Europe, and tends to decrease in coastal regions and at the boundaries of the sampled habitat.

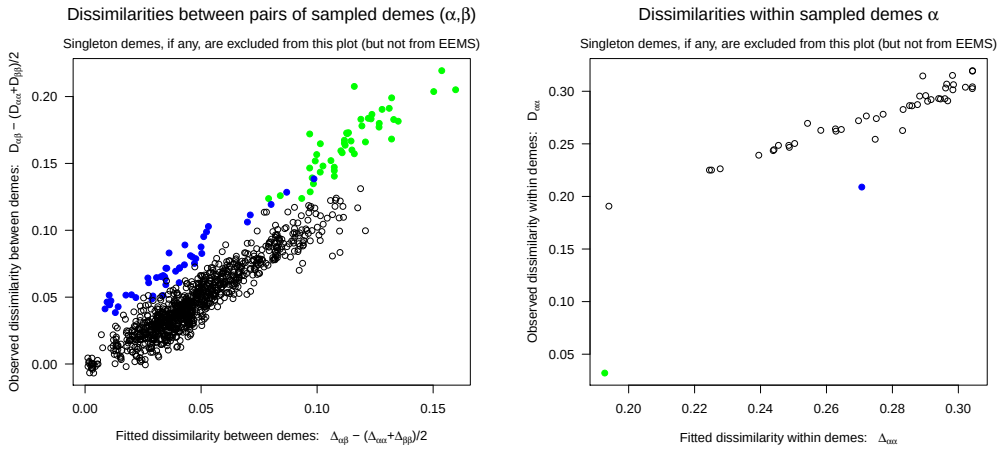

(a)

(b)

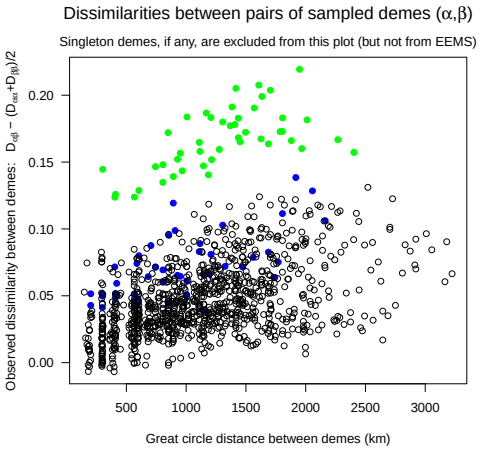

(c)

Supplementary Figure 22 Observed vs fitted genetic dissimilarities, between and within demes on a 15×14 grid, for *Arabidopsis thaliana* in Europe. Singleton demes (those with a single sample) are excluded from the scatter plots. **(a)** Dissimilarities between demes. The fitted values $B_{\alpha\beta} = \Delta_{\alpha\beta} - (\Delta_{\alpha\alpha} + \Delta_{\beta\beta})/2$ comprise the between-demes component of genetic dissimilarity. **(b)** Dissimilarities within demes. The fitted values $W_\alpha = \Delta_{\alpha\alpha}$ comprise the within-demes component of genetic dissimilarity. If the EEMS model fits the data well, we expect a strong linear relationship between the observed and fitted values in both scatter plots. **(c)** Genetic dissimilarities against geographic distances between demes. If isolation by distance (IBD) explains the spatial patterns in the data well, we expect a strong linear relationship between genetic dissimilarity and geographic distance. There are two demes highlighted in blue and green respectively in **Supplementary Figure 21**. They are highlighted in the same colors in the three scatter plots. In (a,c), the colored points correspond to pairs $\langle \alpha, \gamma \rangle$ for each other non-singleton deme γ in the grid. The two diagnostic scatter plots (a,b) suggest that the blue and green demes are not explained well by the fitted EEMS model.